frontiers in Materials

ORIGINAL RESEARCH
published: 03 December 2020
doi: 10.3389/fmats.2020.528590

Surface Functionalization of Three Dimensional-Printed Polycaprolactone-Bioactive Glass Scaffolds by Grafting GelMA Under UV Irradiation

Farnaz Ghorbani[1], *Melika Sahranavard*[2], *Zohre Mousavi Nejad*[2], *Dejian Li*[1], *Ali Zamanian*[2]* *and Baoqing Yu*[1]*

[1] Department of Orthopedics, Shanghai Pudong Hospital, Fudan University Pudong Medical Center, Shanghai, China,
[2] Department of Nanotechnology and Advanced Materials, Materials and Energy Research Center, Karaj, Iran

In this study, bioactive glass nanoparticles (BGNPs) with an average diameter of less than 10 nm were synthesized using a sol-gel method and then characterized by transmission electron microscopy (TEM), differential scanning calorimetric (DSC), Fourier transforms infrared spectroscopy (FTIR), and x-ray spectroscopy (XRD). Afterward, three dimensional (3D)-printed polycaprolactone (PCL) scaffolds along with fused deposition modeling (FDM) were incorporated with BGNPs, and the surface of the composite constructs was then functionalized by coating with the gelatin methacryloyl (GelMA) under UV irradiation. Field emission scanning electron microscopy micrographs demonstrated the interconnected porous microstructure with an average pore diameter of 260 μm and homogeneous distribution of BGNPs. Therefore, no noticeable shrinkage was observed in 3D-printed scaffolds compared with the computer-designed file. Besides, the surface was uniformly covered by GelMA, and no effect of surface modification was observed on the microstructure while surface roughness increased. The addition of the BGNPs the to PCL scaffolds showed a slight change in pore size and porosity; however, it increased surface roughness. According to mechanical analysis, the compression strength of the scaffolds was increased by the BGNPs addition and surface modification. Also, a reduction was observed in the absorption capacity and biodegradation of scaffolds in phosphate-buffered saline media after the incorporation of BGNPs, while the presence of the GelMA layer increased the swelling potential and stability of the composite matrixes. Moreover, the capability of inducing bio-mineralization of hydroxyapatite-like layers, as a function of BGNPs content, was proven by FE-SEM micrographs, EDX spectra, and x-ray diffraction spectra (XRD) after soaking the obtained samples in concentrated simulated body fluid. A higher potential of the modified constructs to interact with the aqueous media led to better precipitation of minerals. According to *in-vitro* assays, the modified scaffolds can provide a suitable surface for the attachment and spreading of the bone marrow mesenchymal stem cells (BMSCs). Furthermore, the number of the proliferated cells confirms the biocompatibility of the scaffolds, especially after a modification process. Cell differentiation was verified by alkaline phosphatase activity as well as the expression of

OPEN ACCESS

Edited by:
Ziyu Wang,
Wuhan University, China

Reviewed by:
Youhong Tang,
Flinders University, Australia
Le Yu,
Ohio University, United States

***Correspondence:**
Baoqing Yu
doctorybq@163.com
Ali Zamanian
a-zamanian@merc.ac.ir

Specialty section:
This article was submitted to Polymeric and Composite Materials, a section of the journal Frontiers in Materials

Received: *21 January 2020*
Accepted: *16 September 2020*
Published: *03 December 2020*

Citation:
Ghorbani F, Sahranavard M, Mousavi Nejad Z, Li D, Zamanian A and Yu B (2020) Surface Functionalization of Three Dimensional-Printed Polycaprolactone-Bioactive Glass Scaffolds by Grafting GelMA Under UV Irradiation. Front. Mater. 7:528590. doi: 10.3389/fmats.2020.528590

osteogenic genes such as osteocalcin and osteopontin. Accordingly, the scaffolds showed an initial potential for reconstruction of the injured bone.

Keywords: additive manufacturing, 3D printing, bioinspired design, functional structures, composites

INTRODUCTION

The severe demand for bone substitutes has led to the development of different alternatives. Herein, surgical procedures, immune rejection, a limited number of donors, and disease transmission, in autogenic and allogenic bone grafts have been terminated to propose new solutions for the regeneration of lesions (Kiernan et al., 2017). Therefore, tissue engineering scaffolds have been proposed for mimicking the extracellular matrix (ECM) and biological performance of native tissue until the cells could well adhere, proliferate, and differentiate as well as facilitate new bone growth (Miszuk et al., 2018). Accordingly, a biocompatible substrate with a proper porous microstructure containing osteoconductive and biodegradable composition, is required.

A variety of studies indicated that hybrid organic-inorganic scaffolds have higher potentials to simulate the natural composition of bone. Accordingly, of a large number of polymers used in bone reconstruction, polycaprolactone (PCL) with its desirable biocompatibility, low degradation rate, high elongation at break, and mechanical properties has been used for the versatile application of repairing damaged bone (Garcia Garcia et al., 2018; Wang et al., 2019b; Lee et al., 2020). However, the lack of osteogenesis in pure PCL resulted in the fabrication of hybrid systems of both organic and inorganic components. Therefore, it was expected that the addition of bioactive inorganic components to a polymeric-based matrix would produce more favorable results. Accordingly, PCL-based scaffolds were printed using FDM technology, so that the matrix was enriched with calcium or strontium ions. Accordingly, the aforementioned ions can exploit bioactivity and induce the potential of osteogenicity with significantly increased alkaline phosphatase activity, osteopontin, and osteocalcin (De Giglio et al., 2018). A study by Lin et al. (Lin et al., 2018) on a hybrid structure composed of PCL and calcium silicate indicated desirable biocompatibility and resilient physical properties with natural bone. Moreover, osteogenic differentiation of the cells, angiogenesis, and bone healing proved the potential of composite scaffolds in bone repairing. Hence, to overcome the limitation of pure PCL for precipitation of the calcium phosphate mineralization, bioactive glass can be considered as a good candidate (Hajiali et al., 2018). Bioactive glass (SiO_2-CaO-P_2O_5) with desirable biocompatibility can interact with physiological fluids for absorbing calcium and phosphate ions, to form hydroxyapatite-like layers, as the main component of natural bone. Moreover, it can also be used as reinforcement in a composite structure, which improves mechanical stability of the scaffolds. Also, its capability for inducing osteogenic differentiation that results in efficient bone healing should not be ignored (Wang et al., 2019a). Previously, a hybrid of PCL and bioactive glass was prepared using electrospinning technology by Hidalgo et al. (Hidalgo Pitaluga et al., 2018). Accordingly, their investigation showed that the addition of bioactive glass to PCL resulted in an increase in tensile strength and the emergence of osteogenic behavior. In a similar research by Long et al. (Long et al., 2015), the presence of bioactive glass in a collagen-based matrix induced a high degree of bioactivity, so that it could be integrated with the surrounding tissue. Notably, one of the strengths of bioactive glass is its antimicrobial activity against a wide range of bacteria and its ability to reduce the risk of pathogens' biofilm production (Drago et al., 2018) under two mechanisms of action as follows: 1) the implantation of BGNPs into a scaffold leads to the exchange of network-modifier ions (e.g., Na^+, K^+, Ca^{2+}) with H^+ or H_3O^+ ions in body fluids. Moreover, this phenomenon will be followed by an increment in pH; 2) the release of silica, calcium, and phosphate ions from bioactive glass increases osmotic pressure by an enhanced concentration of salts that could potentially damage bacterial walls (Ylänen, 2017).

Conventional scaffolding strategies such as solvent casting, electrospinning, phase separation, and freeze-drying produce single homogeneous scaffolds with limited control on microstructure. Accordingly, additive manufacturing technology with the potential of producing the individually designed scaffolds, fabricating the engineered-structure with accurate control on pore size, shape, and interconnectivity, and generating multi-layered and multi-material constructs has found multipurpose applications in the medical field. Nonetheless, the possibility of direct printing in the defective site, increasing the speed of scaffold preparation, and reducing the cost of manufacturing are the other benefits of this technology in biomedical applications. In this method introduced by Hull et al. (Hull, 1986), computer-aided manufacturing (CAM) and computer-aided design (CAD) are used to print synthetic scaffolds, mimic ECM, and provide microenvironments for cell performance, functionalization, vascularization, and finally for the reconstruction of injured sites (Tan et al., 2014). Also, the selective laser sintering printed poly(L, D) lactic acid-bioactive glass scaffolds were evaluated by Salmoria et al. (Salmoria et al., 2018) for the regeneration of bone defects. Accordingly, in this technology, the fabrication of the interconnected porous microstructure with a pore diameter of approximately 200 μm was achieved, while a high level of mechanical strength was observed compared with native bone and desirable cellular interaction. Besides, Rindone et al. (Rindone et al., 2017) in a study evaluated the fused deposition modeling printed PCL-decellularized bone ECM scaffolds. According to their observations, the prepared constructs showed an interconnected porous microstructure with a high degree of accuracy, so that the scaffold geometry precisely matched with the defective site. Furthermore, the osteoinductive behavior of the scaffolds was the strength of this study, which make them

favorable to be applied in the bone healing process. Fused deposition modeling printed scaffolds composed of PCL-polylactic acid indicated about 90% accuracy, which is considered as an essential parameter in medical applications. Additionally, the porous scaffolds could provide a substrate for 3T3 cell adhesion and proliferation, as well as proving their initial potential for clinical applications (Guerra et al., 2018).

Although the application of both PCL and bioactive glass supply the required mechanical strength and osteogenic performance, the hydrophilicity of the 3D printed-PCL-bioactive glass scaffolds can affect cellular interactions, so it needs to be improved. Therefore, to overcome this limitation, the surface of the scaffolds can be modified with hydrophilic components. Gelatin, as a collagen-derived polymer, is a hydrophilic and biodegradable macromolecule that is widely used in tissue engineering. Since gelatin can improve cell adhesion, proliferation, and differentiation through providing the integrin-binding sites (Ghorbani et al., 2018b), it has been considered as a suitable choice for surface modification of the hydrophobic and superhydrophobic constructs. Moreover, the immobilization of gelatin on the PCL scaffolds was focused by Ma et al. (Ma et al., 2005), and the obtained results demonstrated a significant improvement in cell adhesion, spreading, and proliferation. In a similar study performed by Li et al. (Li et al., 2008), gelatin grafting on PCL scaffolds led to a reduction in contact angle, produced hydrophilic surface, and promoted cell attachment and proliferation. In this regard, it should be considered that pure gelatin can form an unstable hydrogel with a low mechanical strength, so to keep its integrity for medical application, it needs modification. Although chemical cross-linking of gelatin with glutaraldehyde, silane coupling agents, and genipin (Tonda-Turo et al., 2011) supply the required mechanical needs, photo-cross-linking showed a rapid and uniform *in-situ* modification, so it is preferred for medical applications. Accordingly, the functionalized type of gelatin is required for photo-cross-linking. Therefore, gelatin methacryloyl (GelMA) with a high potential for reaction with ultraviolet (UV) light and suitable biocompatibility (Bertassoni et al., 2014) have found versatile biomedical applications. Moreover, the concentration of active groups in the polymer and time of UV light irradiation can affect the mechanical strength and stability of the GelMA-contained constructs. According to the observations of Yin et al. (Yin et al., 2018), applying GelMA in composite structures can promote process-ability and shape fidelity. In addition, they also indicated the desirable viability and spreading of the bone marrow stem cells. A study by Wang et al. (Wang et al., 2018) on the stereolithography prepared GelMA-based scaffolds indicated that Young's modulus, cellular adhesion, and proliferation have improved as functions of GelMA concentration; besides, the formed cellular network followed the structure of the 3D printed matrix.

In this study, PCL-bioactive glass scaffolds were prepared using FDM 3D printing technology, and the surface of the constructs was modified with GelMA under UV light irradiation. Also, the prepared matrixes were then evaluated with proper physicochemical and mechanical analyses, to determine the roles of bioactive glass and surface modification on the final properties. In the next step, the scaffolds were cultured with bone marrow mesenchymal stem cells to evaluate cell adhesion, viability, and osteogenic differentiation potential. Finally, the suitable constructs were introduced for further pre-clinical or clinical studies.

MATERIALS AND METHODS

Materials

Gelatin (M_w 40–50 kDa), tetraethylorthosilicate (TEOS, M_w 208.33 gr/mol), calcium nitrate (M_w 236.15 gr/mol), triethyl phosphate (TEP, M_w 182.16 gr/mol), dichloromethane (DCM, M_w 84.93 gr/mol), and nitric acid (0.1M, M_w 63.01 gr/mol) were purchased from the Merck Co. Ltd. (Massachusetts, United States). Methacrylic anhydride (M_w 154.16 gr/mol), lithium phenyl-2,4,6-trimethyl-benzoyl phosphinate, ammonia solution (M_w 17.03), ethanol (M_w 46.07), thiazolyl blue tetrazolium bromide (MTT, M_w 414.32 gr/mol), dimethyl sulfoxide (DMSO, 1X), and *p*-nitrophenyl phosphate (pNPP, tablet) were purchased from the Sigma Co. Ltd. (Massachusetts, United States). Dulbecco's Modified Eagle's Medium (DMEM) was purchased from the Mehregan Biotechnology Co. Ltd. (Alborz, Iran). Fetal bovine serum (FBS) and penicillin-streptomycin were purchased from Gibco-BRL, Life Technologies Co. Ltd. (NY, United States). A Power SYBR™ Green RNA-to-CT™ 1-Step Kit was purchased from the Thermo Fisher Scientific Co. Ltd. (Massachusetts, United States). Phosphate buffered saline (PBS, powder, pH 7.2–7.4) and simulated body fluid (SBF, pH 7.2–7.4) were purchased from the Aprin-ATD Co. Ltd. (Tehran, Iran). An alkaline phosphatase kit (ALP) was purchased from the MAN Co. Ltd. (Tehran, Iran). Aqueous solutions were prepared with deionized (DI) water. All reagents were used without further purification.

Synthesis of Bioglass Nanoparticles

BGNPs ($64SiO_2.28CaO.8P_2O_5$) were synthesized via the sol-gel method according to previously published research (Pourhaghgouy et al., 2016). Briefly, TEOS (43.67 gr) and DI-water (174.76 ml) were blended with a mixture of ethanol (87.33 ml) and nitric acid (5.5 ml of 2M) under gentle stirring. After 30 min, TEP (8.38 ml) and calcium nitrate tetrahydrate (20.16 gr) were blended with the prepared solution and stirred for 30 min. This procedure was followed by another 1 h stirring to age the solution. Then, the drop-wize addition of ammonia solution to the stock solution led to the conversion of the sol to a gel. Dried powder was collected by putting the gels in an oven (VOcool, Memmert, Germany) at 70°C for 3 d. Finally, the obtained powder was heated at a rate of 3°C/min at 700°C for 2 h and was slowly cooled down.

Synthesis of GelMA

GelMA was prepared according to the investigation of Correia et al. (Correia et al., 2016). Briefly, gelatin was dissolved in PBS solution with a concentration of 10%(w/v), and methacrylic anhydride was mixed with a solution at 40°C under 1 h vigorously stirring. The final solution was dialyzed against

DI-water for 4 d at ambient temperature and the products were transferred into a freeze-dryer (FD-10, Pishtaz Engineering Co. Iran) and lyophilized at the temperature of −58°C and pressure 0.5 torr for 48 h.

Preparation of Nanocomposite Scaffolds

PCL solution in DCM with a concentration of 5% (w/v) was made on a magnetic stirrer for 3 h at 40°C, then BGNPs with a PCL: BGNPs ratio of 70:30 was added to the solution and the mixture was allowed to stir for 1 h until a milky color suspension was obtained. Afterwards, the milky suspension was cast onto a glass petri dish and kept in a clean environment at room temperature to dry. The dried film was cut into 5 mm slices to be ready for use in the printing process. 3D printed constructs were designed using Rhinoceros (Version 5.0 SR8; McNeel, Seattle, WA, USA) and then, by using Ultimaker Cura (Version 3.6.0) the final file was saved as a G-code file in order to be readable by a Bioprinter machine. Accordingly, composite slices were loaded in the cartridge of the 3D BIOPRINTER N2 (3DPL Co. Ltd. Tehran, Iran) to print the scaffolds under a temperature of 90°C, pressure of 6 bar, and speed of 2 mm/s. The layer-by-layer extruded materials deposited on the bed with the designed angle of 0 and 90° and a layer thickness of 0.4 mm. Finally, the obtained scaffolds were dried in an oven at 36 ± 0.5°C for 24 h.

Surface Modification

GelMA was dissolved in DI-water to achieve a solution with a concentration of 1%(W/V), and after complete dissolution, photoinitiator lithium phenyl-2,4,6-trimethyl-benzoyl phosphinate with a concentration of 0.05% (w/v) was added under gentle stirring at 40°C. After the preparation of solutions, the scaffolds were immersed in the solutions for 3 min, then the surface of the scaffolds was irradiated by UV-light (365 nm) with the irradiation intensity of 2 W/cm^2 for 2 min and dried in an oven at ambient temperature.

Table 1 Indicated abbreviation of names and details about the fabrication of scaffolds. The short name was selected based on applied materials and fabrication technology.

Characterization

The morphology of the BGNPs was observed by transmission electron microscope (TEM, CM120, Philips Co., Netherlands) at a voltage of 100 kV. So the particles were dispersed in the ethanol, and BGNPs-contained drops were deposited in carbon-coated copper grids.

The microstructure of 3D-printed scaffolds was observed by a field emission scanning electron microscopy (FE-SEM, MIRA3, TESCAN Co., Brno, Czech Republic) at an accelerating voltage of 15 kV. The constructs were sputter-coated with a thin layer of gold to improve conductivity. The porosity of the samples was calculated by **Eqs 1–4** (Ghorbani and Zamanian, 2018). Where V_P, V_S, ρ_s, and ε are the volume of the scaffold pores, the volume of the scaffold skeleton, the density, and the porosity, respectively. Briefly, the printed scaffolds were immersed in a bottle of ethanol (ρ_e, W_1). Then, the bottle of ethanol and a bottle of the scaffold was measured separately (W_2, W_3, respectively).

$$V_S = (W_2 - W_3 - W_S)/\rho_e \quad (1)$$

$$V_S = (W_1 - W_2 + W_S)/\rho_e \quad (2)$$

$$\rho_S = W_S/V_S = W_{Spe}/(W_1 - W_2 + W_S) \quad (3)$$

$$\varepsilon = V_p/(V_p + V_S) = (W_2 - W_3 - W_S)/(W_1 - W_3) \quad (4)$$

The variation of surface roughness after modification was assessed by an atomic force microscopy (AFM, Rasterscope C26, DME Co., Denmark) technique by a STM mode t with a resonance frequency of 50–105 kHz.

The thermal behavior of BGNPs and the calcination temperature were determined via simultaneous thermal analysis (STA, PL-STA-1640, Polymer Laboratories, Stanton. Redcraft, UK). Differential thermal analysis (DTA) curves were recorded at the heating rate of 20°C/min from ambient temperature to 1000°C.

Chemical characterization was performed with a Fourier transforms infrared spectroscopy (FTIR, Nicolet Is10, Thermo Fisher Scientific, United States) system in the wavenumber of 400–4000 cm^{-1} with a resolution of 4.0 cm^{-1} and 8 scans.

Phase analysis of the samples was done with an x-ray powder diffractometer (XRD, PW3710, Philips Co., Netherlands). The spectra were obtained in the range of 2θ (10–60°) using Cu-Kα (λ = 1.5418 A°) radiation under the operating conditions of 40 kV and 30 mA. XRD patterns were compared with JCPDS standards to identify the crystalline phases.

The compressive strength of 3D-printed scaffolds was measured by a compression strength test system (STM 20, Santam Co., Tehran, Iran) using 100 N load cell under a crosshead speed of 0.5 mm/min.

The wettability of hybrid scaffolds was evaluated by contact angle measurements using the sessile drop method at an ambient temperature (DSA 100, KRÜSS GmbH Co., Hamburg, Germany).

The swelling ratio of the constructs was determined after soaking the constructs in the PBS solution at 37 ± 0.5°C under a shaking speed of 30 rpm. Accordingly, the weights of the constructs were measured after 3, 6, 12, and 24 h immersion (W). The absorption capacity was calculated according to **Eq. 5** (Nandagiri et al., 2011), while W is the initial dry weight of constructs.

TABLE 1 | Details about the fabrication of scaffolds.

Code	Composition	BGNPs concentration (wt%)	Fabrication technology	Modification technology
PC	PCL	0	FDM 3D-printing	—
PCB	PCL-BGNPs	30	FDM 3D-printing	—
PCBG	PCL-BGNPs	30	FDM 3D-printing	Immobilization of GelMA under UV light

$$\text{Swelling ratio}\,(\%) = [(W - W_0)/W_0] \times 100 \quad (5)$$

Biodegradation rate of the scaffolds was determined through the immersion of constructs in the PBS solution at 37 ± 0.5°C under a shaking speed of 30 rpm. Accordingly, the dry weight of constructs was measured weekly, and the media was refreshed at each time interval. The change in weight was evaluated and biodegradation was calculated according to **Eq. 6** (Pourhaghgouy et al., 2016), while W is the initial dry weight of constructs.

$$\text{Biodegradation ratio}\,(\%) = \left|\left[(W - W_0)/W_0\right]\right| \times 100 \quad (6)$$

The potential of 3D-printed scaffolds for biomineralization of hydroxyapatite-like layers was determined through the immersion of constructs in the SBF solution at 37 ± 0.5°C under a shaking speed of 30 rpm for 4 weeks. Every other day, the media was refreshed, and at the end, the morphology of the precipitated minerals was observed by FE-SEM, and the phase analysis of the deposited layer was conducted by x-ray diffraction.

Cell-Scaffolds Interactions

The cell-scaffolds interaction was evaluated after the sterilization of the scaffolds with sterile PBS and penicillin-streptomycin at an ambient temperature. Then, rat bone marrow mesenchymal stem cells (BMSCs) with a concentration of 5×10^4 cells/ml were seeded on the sterilized samples in the presence of cell culture media (DMEM with 10% FBS and 100 mg/ml penicillin-streptomycin) and incubated at 37 ± 0.5°C, 5% CO_2, and 95% humidity for 3 d. Finally, to observe the morphology of adhered cells with FE-SEM images, the scaffolds were washed with PBS and fixed with 3% glutaraldehyde solution and 1% osmium tetroxide followed by dehydration with ethanol solutions of ascending concentrations.

The viability of the cells was determined with an MTT assay after 3, 7, and 14-days cultures. Accordingly, the media was removed, and both the MTT (3-{4,5-dimethylthiazol-2yl}-2,5-diphenyl-2H-tetrazolium bromide) solution and fresh media with a weight ratio of (1:5) was replaced. After incubation, the formazan was dissolved in DMSO and the optical density was measured at the wavelength of 570 nm.

The level of differentiation and osteoblastic behavior of cultured cells after 3, 7, and 14 days and the release of *p*-nitrophenol from *p*-nitrophenyl phosphate (*p*-NPP) was measured to determine the ALP activity. Accordingly, the proliferated cells were lyzed by the addition of a 0.1% Triton X-100 lysate in the presence of a *p*-NPP solution at 37 ± 0.5°C and the ALP kit was applied. ALP activity was determined by measuring *p*-NPP absorbance at the wavelength of 405 nm after stopping the reaction with NaOH (1N).

Quantitative RT-PCR was performed after RNA extraction for determining the level of osteocalcin (OC) and osteopontin (OP) after 7, 14, and 21 days of culture. Accordingly, 0.4 μL of 125X RT Enzyme Mix, 5 μL of the RNA template, 25 μL of 2X RT-PCR Mix, 1.5 μL of 20 μM forward and reverse primers, and nuclease-free water were added to a total volume of 50 μL to determine the level of each protein. The below specific sequence was used for the determination of differentiation. The thermal cycles were done in 3 steps, including reverse transcription at 48°C for 30 min, enzyme activation at 96°C for 15 s, and PCR amplification at 96°C for 15 s and 60°C for 60 s. The obtained values were normalized with the housekeeping gene GAPDH mRNA (Hs99999905_m1).

OC → forward: GTGCAGCCTTTGTGTCCAAG, reverse: TCCTGAAAGCCGATGTGGTC.

OP → forward: ATGGTGCATACAAGGCCATC, reverse: TCGGAATGCTCATTGCTCTC.

Statistical Analysis

The results of each test were repeated 5 times and collected in the Microsoft Excel 2016 software. The reported value is as the mean ± standard deviation of five experiments and was processed using the Microsoft Excel 2016 software. The significance of the average values was calculated using a standard software program (SPSS GmbH, Munich, Germany), and $p \leq 0.05$ was considered significant.

RESULTS AND DISCUSSION

Characterization of BGNPs

TEM micrographs of BGNPs are presented in **Figure 1A**. According to the observations, the sol-gel method led to the formation of BGNPs, so that they showed an average size of 10 nm. Also, the aggregation of particles may arise from the cluster formation of nanoparticles owing to a high surface area (Hong et al., 2008).

The mass reduction rate of BGNPs, as a function of temperature, is indicated in **Figure 1B**. As shown, heating the samples from ambient temperature up to 1000°C resulted in a 64% reduction of the weight. The loss of the mass from ambient temperature up to 240°C may be attributed to the removal and volatilization of both physically and chemically adsorbed mass. Correspondingly, chemically adsorbed water can be observed due to the condensation of catalysts or precursors. The weight reduction from 240 to 550°C can be related to the loss of organic precursors such as alkoxides in the chemical composition of the sample (Sharifi et al., 2016). The weight reduction from 550 to 700°C can be corresponded to nitrate decomposition and condensation of the silanol groups. All the observed peaks in the diagram were endothermic and the lack of an exothermic peak can be considered as a sign of superficial crystallization (Heidari et al., 2018). Sudden weight reduction and a sharp endothermic peak in the DTA diagram from 550 to 600°C can be an indicator for thermal decomposition as well as the existence of metal nitrate (Jones et al., 2006). By increasing the heating temperature, no significant changes have been observed in the diagram after 700°C, which is the sign of stabilization. In this regard, similar results were observed in other studies (Oki et al., 2004; Sharifi et al., 2016). Moreover, other investigations indicated that an increase in the stabilization temperature led to a reduction in the number of hydroxyl groups in the chemical composition of BGNPs, which are necessary for the nucleation of

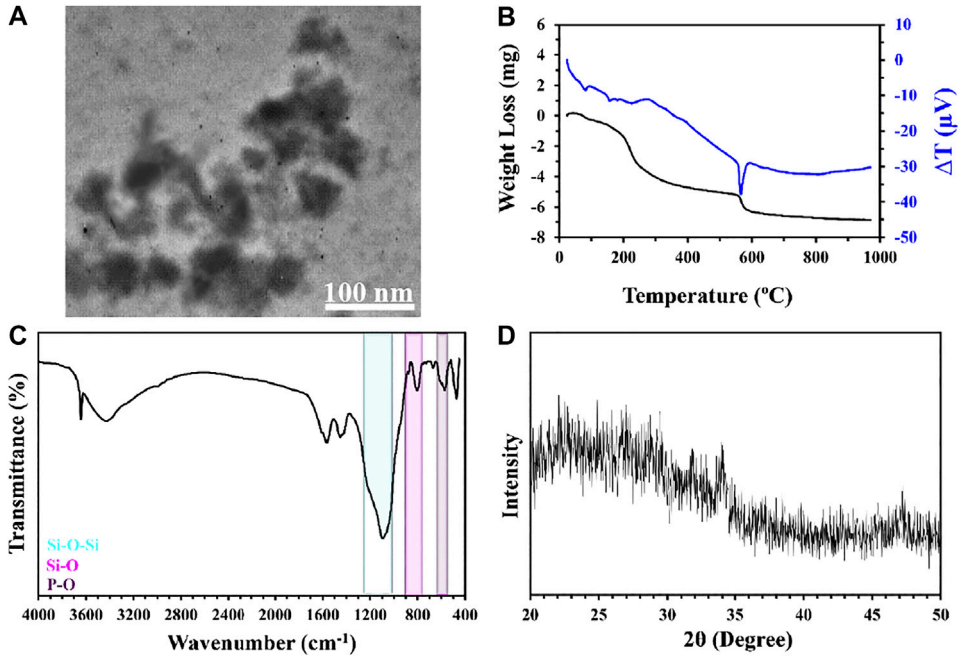

FIGURE 1 | TEM image **(A)**, DSC thermograms **(B)**, FTIR spectra **(C)**, and XRD spectra **(D)** of bioglass nanoparticles.

hydroxyapatite-like layers, and for reducing the bioactivity potential of synthesized particles (Hench et al., 1998; Kokubo, 2008; Liu et al., 2009).

The chemical composition of BGNPs was evaluated using FTIR spectra, as indicated in **Figure 1C**. Accordingly, asymmetric and symmetric stretching vibrations of the Si-O-Si bond can be observed at 1,212 and 1,100 cm^{-1}. Also, the peaks appeared at 877 and 801 cm^{-1} to Si-O bonds and both bridging and non-bridging oxygen in its structure. The bending vibration of the P-O was also detected at 671 and 570 cm^{-1}. The phase analysis with XRD spectra (**Figure 1D**) demonstrated the amorphous structure of BGNPs, since no sharp peaks appeared in the spectra between 2θ angles of 20–50°.

Characterization of Scaffolds

Morphology Observation and Surface Topography

Various investigations indicated that the microstructure of scaffolds, i.e., porosity, pore size and shape, and interconnectivity are the most essential criteria to support 3D cell growth, induce vascularization, and regenerate defective sites (Park et al., 2018a). Among a number of technologies proposed to fabricate scaffolds, 3D printing has been known as the most accurate technique that provides an opportunity to design scaffolds based on biomimicry, autonomous self-assembly, and the requirements of the target tissue. Spatial control on the pore parameters, such as porosity, interconnectivity, pore size and shape, potential to print multi-material, and multi composition scaffolds as well as printing the cells and biological/pharmaceutical agents, reproducibility, fabrication of patient-specific structure, and the possibility of direct printing in defective sites all play important roles in the dominance of 3D printing over traditional methods. Also, another study indicated that controlling and engineering the microstructure of the scaffolds can positively affect cellular adhesion, proliferation, and migration, as well as promoting the interchange of nutrition and waste by-products (Yan et al., 2005). In this state of art technology, 3D designed files were used for layer-by-layer printing of the structure. In this regard, nowadays, different methods of acellular 3D printing technologies, including stereolithography, selective laser sintering, and fused deposition modeling, are used in the fabrication of scaffolds. In this investigation, FDM technology was also applied for the fabrication of scaffolds. Notably, an FDM 3D printer is one of the most common and cost-effective setups that works based on layer-by-layer extruding of the molten thermoplastic filaments (Zein et al., 2002). Herein, the adjusted angle of the printed scaffolds with bed and layer thickness can affect dimensional accuracy and the pore microstructure (Wu et al., 2015). Notably, printing temperature has been known as an effective factor on the final structure, in a way that an increase in temperature leads to the volatilization and reduction in viscosity and strength, so it can prevent dimensional accuracy (Yang et al., 2017).

Figure 2 and **Table 2** indicate FE-SEM micrographs and surface roughness of the PCL-based scaffolds that were printed using FDM technology and then modified with GelMA under UV irradiation. Based on these observations, all the scaffolds showed some parallel aligned filaments in both horizontal and vertical directions, continuous layer-by-layer extruding of the filaments, and finally in the formation of an interconnected microtubule-like microstructure with low shrinkage, compared to the 3D-designed file. The average porosity of the prepared scaffolds was 60%, and the 3D-printed construct showed a high degree of

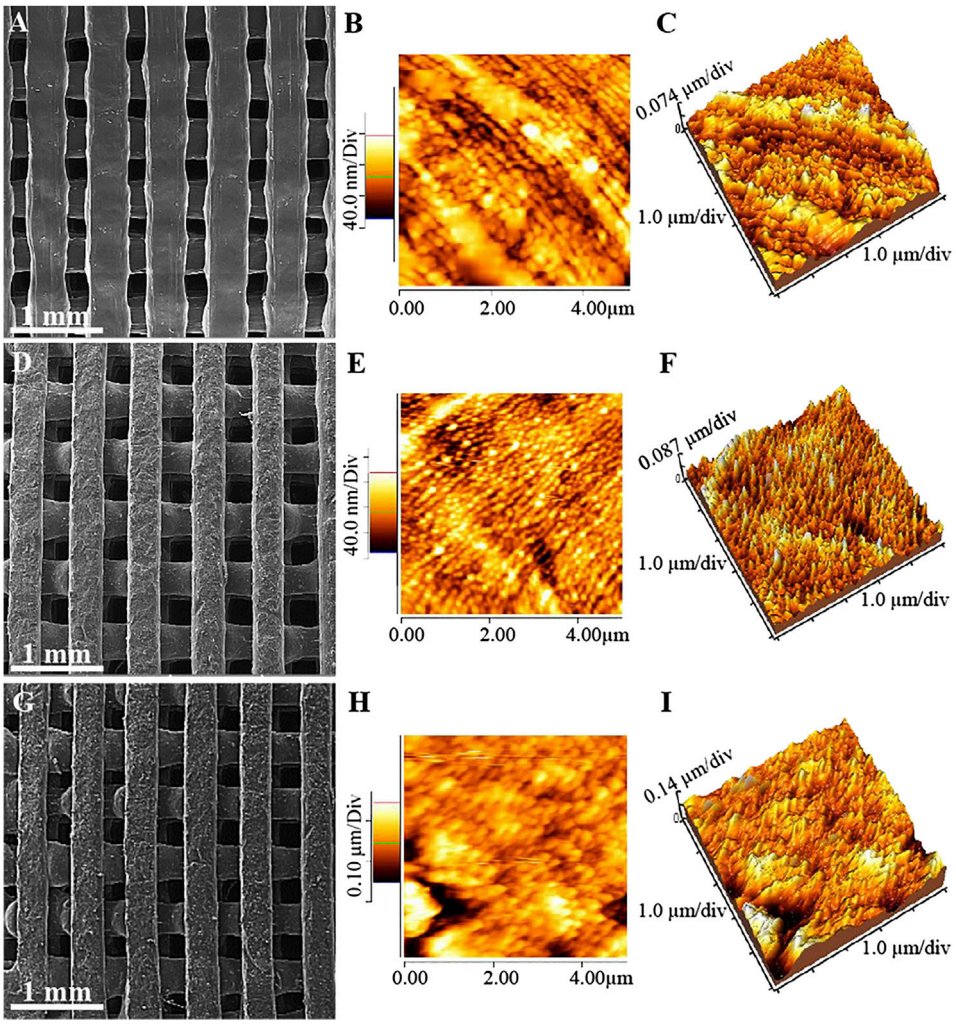

FIGURE 2 | FE-SEM micrographs **(A)**, **(D)**, **(G)**, and both 2 dimensional and 3 dimensional AFM images **(B)**, **(C)**, **(E)**, **(F)**, **(H)**, and **(I)** of PC **(A)**–**(C)**, PCB **(D)**–**(F)**, and PCBG **(G)**–**(I)** scaffolds.

TABLE 2 | Surface roughness of PC, PCB, and PCBG scaffolds.

Code	Rp-v (nm)	Rms roughness (Rq, nm)	Average roughness (Ra, nm)
PC	147.8	17.84	14.32
PCB	175	21.31	16.62
PCBG	274.6	33.27	24.26

porosity for cellular interactions and bone repair (Unnithan et al., 2015). Different studies indicated that the porosity in the range of 50–60% would be suitable for cell adhesion, proliferation, migration, differentiation and finally, for reconstructing injured bone. However, the effect of porosity on mechanical strength and maintaining the integrity of constructs is an important factor that should not be ignored. Moreover, PC scaffolds indicated a pore size of ~220 µm and a strand width of ~420 µm, while the addition of BGNPs resulted in a higher uniformity of microstructure as well as homogeneous distribution of BGNPs in the PCL matrix, which consequently increased the surface roughness parameters (**Table 2**). Accordingly, several similar results were reported in a study by Jeon et al. (Jeon et al., 2019) after the addition of silica particles to the PCL matrix. An increase in pore size (~300 µm) and a reduction in strand width (~360 µm) were also observed after the addition of BGNPs to PCL strands. In addition, a narrower strand width can be responsible for the enhancement of pore size in PCB constructs. The fabrication of 3D-printed scaffolds with spherical pores with a size of 300 µm, which is similar to the PCB scaffold results, resulted in the promotion of cell growth and the regeneration of osteochondral defects in rabbits (Liu et al., 2019). Based on a study by Gutta et al. (Gutta et al., 2009), a pore size less than 150 µm is not preferred for bone regeneration, while a pore size higher than 400 µm cannot show a perfect *in-vivo* osteogenesis performance (Zhang et al., 2014; Pati et al., 2015). Compared with

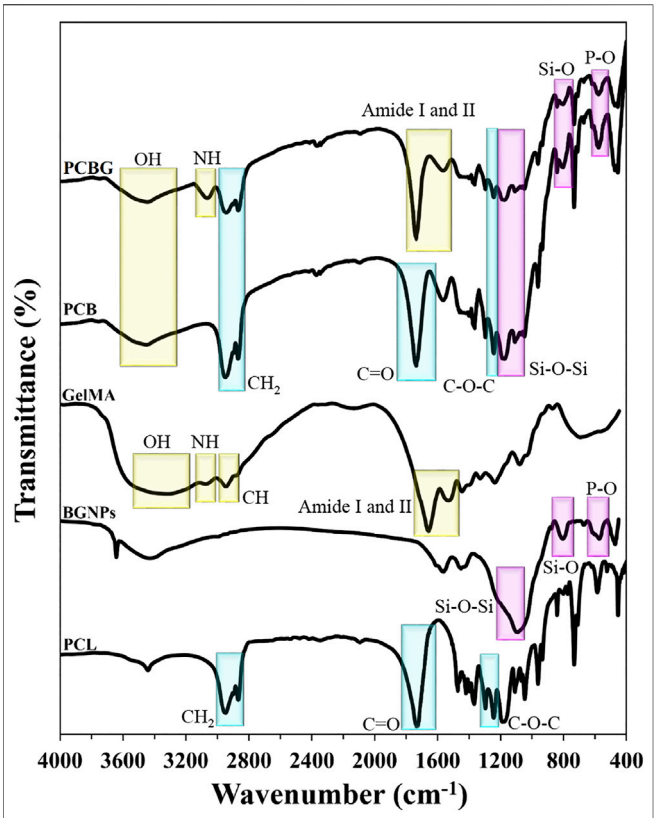

FIGURE 3 | FTIR spectra of raw materials and composite structures.

other pieces of literature, the PCL-based scaffolds have been designed with a suitable pore size for bone tissue engineering applications, which are expected to support oxygenation, cell proliferation, migration, vascularization, and osteogenic expression.

Surface modification plays a decisive role in directional growth, proliferation, and differentiation of the cells. So, the PCB scaffolds were modified through grafting the GelMA on the surface of constructs under UV light irradiation. Moreover, the direct modification of scaffolds was performed through photo-induced cross-linking and grafting the GelMA onto the surface with no surface pre-activation, to control the harmful effect of the pre-activated surface, and to reduce the processing step, time, and cost. Since the GelMA solution has a relatively high viscosity, it cannot be diffused inside the pores within 3 min of immersion time, so physical gelation will occur on the surface and the hydrogel will be cross-linked and grafted on the surface after the emission of UV lights. After the modification of the surface, a homogeneous layer of GelMA has been observed on the surface of the synthetic matrixes, which had no significant effect on the microstructure of the pores. However, measuring the surface roughness determined that roughness parameters have increased after grafting GelMA on the surface of the PCB scaffolds, as presented in **Table 2**. Since the rough surface can provide more anchorage sites for the cells as well as improving physical bonding (Su et al., 2011), it is expected that better cell-scaffold interactions will occur in the PCBG constructs compared with the PC and PCB ones. Besides, the average roughness of stands was in the nano-scale range, and according to the previously published literature, nano-scale roughness could lead to the improved differentiation of the cells and the expression of the genes (Thomas et al., 2002; Lee et al., 2004). So, the promoted osteogenic performance is expected after surface modification.

Chemical Characterization

FTIR spectra of raw materials and composite scaffolds are shown in **Figure 3**. The sharp peaks at 2,948 and 2,866 cm^{-1} were observed from the FTIR spectrum of the PCL sample that can be attributed to CH_2 stretching vibration. Moreover, C=O, (C-O, C-C), and C-O-C stretching vibrations (carbonyl and etheric functional groups) in the chemical composition of PCL can be detected at 1,723, 1,296, and 1,242 cm^{-1}, respectively. The characteristic peaks to identify BGNPs are explained in *Characterization of BGNPs*.

In this study, the molar ratio of MAA to free NH2 groups for the preparation of GelMA has been set as 2:1 according to the study by Correia et al. (Correia et al., 2016). In addition, photo-cross-linking the GelMA under UV rays leads to the observation of better biocompatibility and improves the cell-scaffolds interactions besides increasing the long-lasting coating layers and enhancing the mechanical stability (Yue et al., 2015). In the case of GelMA, the appeared peak around 3,300–3,500 cm^{-1} is an indicator of OH. The appeared peaks at 3,076 and 2,943 cm^{-1} can also be assigned to NH stretching vibrations and saturated CH, respectively. Moreover, the observed peak between 1,700–1,600 and 1,565–1,525 cm^{-1} is an indicator of amide I and II, respectively.

The PCB scaffolds FTIR spectra proved the presence of BGNPs in the PCL strands through observing the related peaks of Si-O-Si, Si-O, and P-O stretching vibrations. After the modification of the surface with GelMA, the intensity of the peaks assigned to PCB reduced. The oxygen-containing functional groups in the chemical composition of the scaffolds like the carbonyl group can provide binding sites for GelMA grafting through the polar interactions or hydrogen bonding (Shen et al., 2007). Accordingly, new peaks are signs that the GelMA has appeared in the FTIR spectra of the modified samples and has also proven that the GelMA has grafted onto the surface.

Mechanical Behavior

The mechanical behavior of tissue engineering scaffolds can be affected by various kinds of parameters, including chemical composition, porosity, pore size and shape, and interconnectivity of the pores. Accordingly, the mechanical strength of reconstructive substitutes play a vital role in bone repair, so the prepared constructs should be strong enough to tolerate the applied stresses and to keep stability. On the contrary, they need to be porous to support cellular diffusion, fluid and oxygen transfer, and remove cellular by-products (Chen et al., 2018). Besides, the mechanical stability of the scaffolds have shown a decisive effect on cell activity and the final morphology, since motility in the actin–cytoskeleton controls

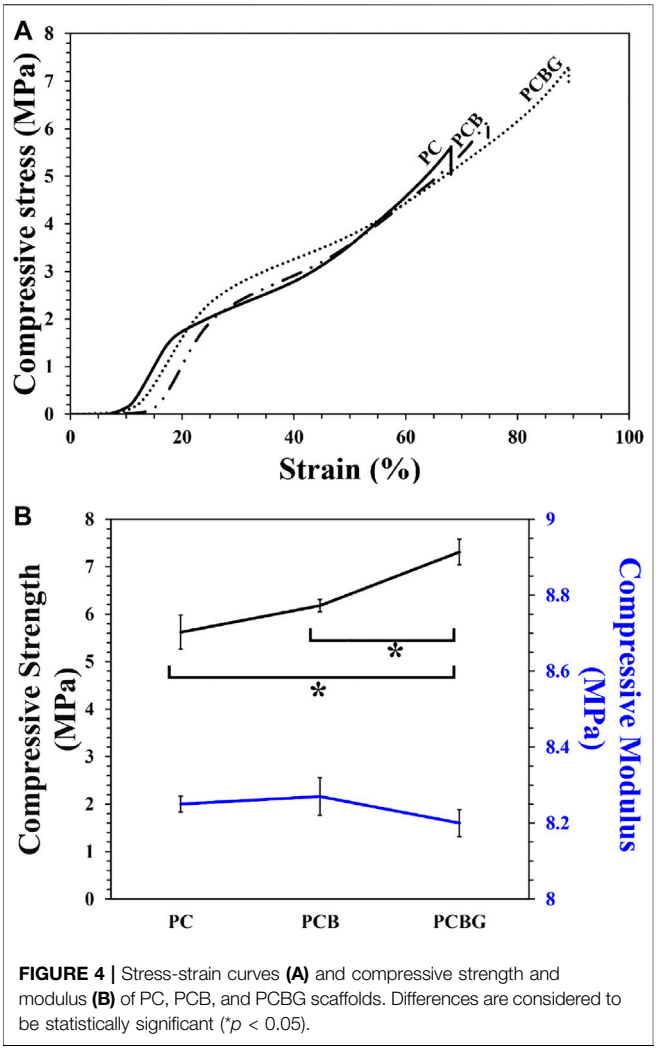

FIGURE 4 | Stress-strain curves **(A)** and compressive strength and modulus **(B)** of PC, PCB, and PCBG scaffolds. Differences are considered to be statistically significant (*$p < 0.05$).

the osteogenic differentiation by the extracellular signal regulated kinase activity, and the mitogen-activated proteinkinase are also dependent on the elastic modulus (Khatiwala et al., 2007). Recently, a wide range of studies have focused on hybrids of the organic-inorganic constructs to prevent stress-shielding using some polymeric biomaterials, by simulation of natural bone composition, and inducing bioactivity and chemical bonding ability with natural bone with the use of bioactive ceramics (Hench, 2015). Previous investigations demonstrated that the FDM-printed scaffolds provided suitable mechanical strength for the regeneration of the bone lesions (Korpela et al., 2013). Accordingly, in this study, the mechanical behavior of 3D-printed constructs composed of PCL and BGNPs, was evaluated and finally, we focused on the role of surface modification in the improvement of mechanical strength. **Figure 4A** shows the stress-strain curves of 3D-printed scaffolds, and both compressive strength and modulus are indicated in **Figure 4B**. Compared with PC scaffolds, PCB and PCBG exhibited higher strengths, which may be attributed to the addition of BGNPs and the modification of the surface with GelMA. Higher surface area in stress-strain curves demonstrated that PCBG constructs have high levels of toughness compared with the PC and PCB constructs, since a high level of energy needs to be absorbed for plastic deformation and the final fracturing. Besides, although the addition of BGNPs led to an increase in pore size and a reduction in strand width, it could act as a reinforcement of the composite structure and for improving the compressive strength, which arises from the stiffer mechanical behavior of ceramic-based biomaterials. However, there were no significant differences between measured values. Correspondingly, these observations are in agreement with the reported values in other pieces of literature (Jose et al., 2009). In contrast, the modification of the surface with GelMA resulted in 1.4 and 1.2 times more significant enhancement in compressive strength of PCBG matrixes compared with the PC and PCB

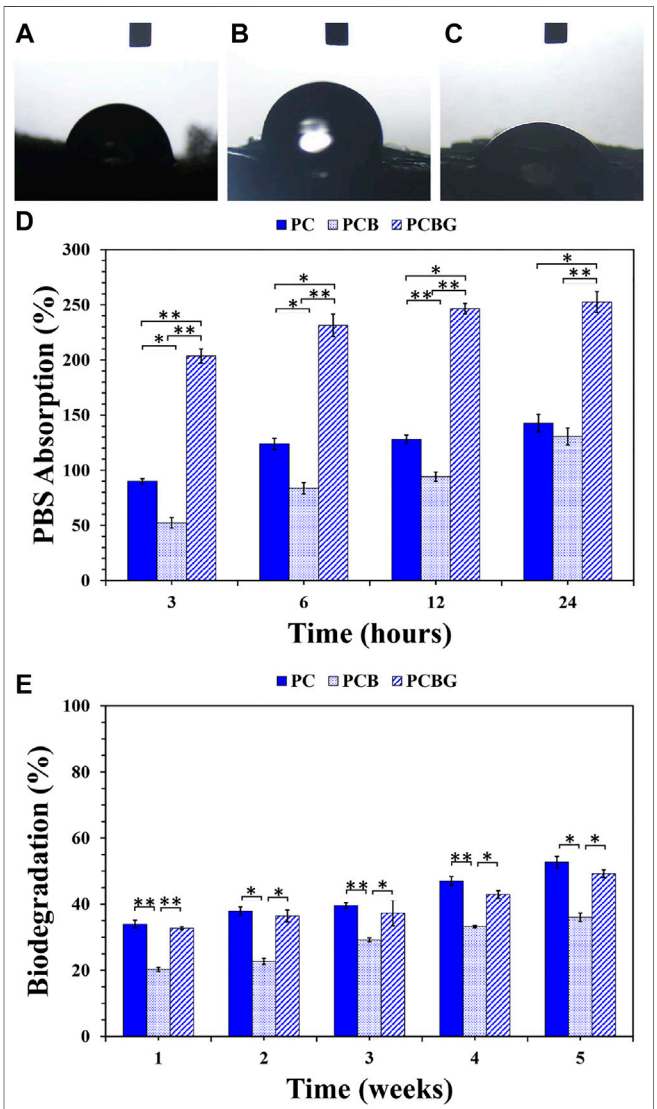

FIGURE 5 | Water-drop contact angle of PC **(A)**, PCB **(B)**, and PCBG **(C)** constructs. The PBS absorption capacity as a function of times **(D)** and a 5-weeks biodegradation ratio **(E)** of 3D-printed matrixes. Differences are considered to be statistically significant (*$p < 0.05$) and very statistically significant (**$p < 0.005$).

matrixes, respectively. However, a slight reduction was also observed in the compressive modulus of PCBG scaffolds compared with PC and PCB, showing a reduction in elastic behavior and a lower resistance to plastic deformation of the constructs. However, these differences were not statistically significant.

Absorption Capacity and Biodegradation

The capability of scaffolds to interact with water molecules is considered a critical factor in tissue engineering, which can be affected by a variety of factors such as chemical composition and porous microstructure. (Pan and Ding, 2012). Since at the early stage of healing, fluid flow is a necessity for supplying the nutrient requirements of the cells, the ability of scaffolds to absorb water molecules is important for reconstruction after injury. According to various investigations, hydrophilic scaffolds with interconnected and tubular pore channels facilitate the capillary action and promote cell-scaffolds interactions, the diffusion of nutrients, secretion of ECM, and finally, tissue ingrowth (Ding et al., 2018; Park et al., 2018c). Moreover, the studies by Siri et al. and Park et al. (Siri et al., 2010; Park et al., 2018b) proved that hydrophilic surfaces provide an adhesive ligand in the basement membrane through the absorption of some proteins such as laminin and supply a better substrate for cell adhesion.

The wettability of the scaffolds, which is an effective factor on cell adhesion and proliferation, was determined using a water-drop contact angle test (sessile drop method) (Huang et al., 2018), and the results are presented in **Figures 5A–C**. Accordingly, the PC, PCB, and PCBG constructs indicated the contact angles at approximately 84.53, 99.21, and 39.87°, respectively. The measured values indicated a lower level of hydrophilicity after the addition of BGNPs as well as the improvement of wettability after surface modification with GelMA. The enhancement of hydrophilicity and the reduction of the contact angle below 40° made the modified scaffolds suitable for the interaction with the cells and the promotion of regeneration since the contact angle (Lin and Fu, 2016).

The PBS absorption potential of 3D-printed scaffolds is presented in **Figure 5D**. According to the measured values, all the scaffolds showed a degree of tendency to interact with water molecules, so that a direct relationship was observed between the time of enhancement and the absorbed PBS. In all the samples, a high water uptake was observed during the first 3 h that was followed by a steady gradient to 24 h. However, PCB constructs showed a higher slope in water uptake compared to the other samples within 24 h. Although both PCL and BGNPs have hydrophobic natures, which is not an appropriate property for cell performance, the tubular porous microstructure of scaffolds and a higher surface area/volume ratio are considered responsible factors for the absorption capability of the scaffolds (Prabha et al., 2018) According to a previous study, directional pore channels can facilitate fluid transfer and also improve the absorption rate compared with the prepared scaffolds by other technologies with randomly-oriented microstructures, which finally affect the regeneration process (Yetiskin and Okay, 2019). Based on the obtained results, although PCB scaffolds showed a larger pore size, the addition of BGNPs to PCL matrixes led to a significant reduction in the absorption capacity in all time intervals, in a way that some statistically considerable differences were observed in PBS uptake after 12 and 24 h. This phenomenon may arise from decreasing the interaction of scaffolds with PBS molecules owing to the formation of a barrier by BGNPs on the surface of PCL strands. The possible interaction of BGNPs with PCL functional groups, which play a role in the absorption of PBS molecules, can be considered as a reason for the reduced PBS absorption (Videau and Dupuis, 1991). Although a reduction in adsorption capacity was observed after the addition of BGNPs, its decisive role in osteogenic differentiation led to us ignoring its slight influence on hydrophilicity (Zahedi Tehrani et al., 2018). After the functionalization of the surface, the existence of GelMA clearly improved the absorption ratio owing to the promoted hydrophilicity that arises from the enriched surface with hydrophilic functional groups such as hydroxyl and amide and possible hydrogen bonding with water molecules (Correia et al., 2016). Several significant statistical differences were observed in the swelling capacity of the PCBG scaffolds compared with the other groups. The same results were also observed in a study by Tsai et al. (Tsai et al., 2011) after surface functionalization with hydrophilic functional groups. Accordingly, the scaffolds with a higher PBS uptake have decisive potentials to absorb proteins and improve the 3D cell spreading modification of the PCL surface with gelatin. Moreover, in the investigation of Xiang et al. (Xiang et al., 2018), an enhancement in hydrophilicity and swelling capacity was demonstrated. In another study by Zhu et al. (Zhu et al., 2004), grafting the gelatin on the surface of scaffolds promoted PBS uptake by aminolysis reactions.

Tissue engineering scaffolds should provide a substrate for cell functionality. Herein, non-degradable or rapid-degradable constructs cannot be considered as good candidates, since a balance between regeneration and biodegradation is required (Boccaccini and Ma, 2014). Chemical composition and additives, level of hydrophilicity, glass transition temperature, morphology and dimension of constructs, molecular weight and molecular weight distribution of the applied materials, porosity characteristics, and target tissue can determine the rate of biodegradation, which are some considerable issues in designing the scaffolds (Anderson and Shive, 2012).

Figure 5E presents the biodegradation ratio of 3D-printed scaffolds after a 5-week period of immersion in the PBS solution. According to the observations, scaffolds could keep their integrity during a 5-weeks experiment, and less than approximately 50% of the scaffolds were degraded. In addition, it should be considered that the tubular porous microstructure of 3D-printed scaffolds may increase the long-lasting constructs compared to the other manufacturing techniques owing to a higher mechanical strength and resistance to collapse resulting from the water-scaffold interactions (Deville, 2017). The results indicate that the addition of BGNPs to PCL led to a significant reduction in the biodegradation ratio. Accordingly, this phenomenon may be attributed to a lower hydrophilicity and higher mechanical strength of PCB scaffolds compared with PC scaffolds. After the surface modification, a higher degradation was observed compared with PCB scaffolds. Hydrophilic functional groups

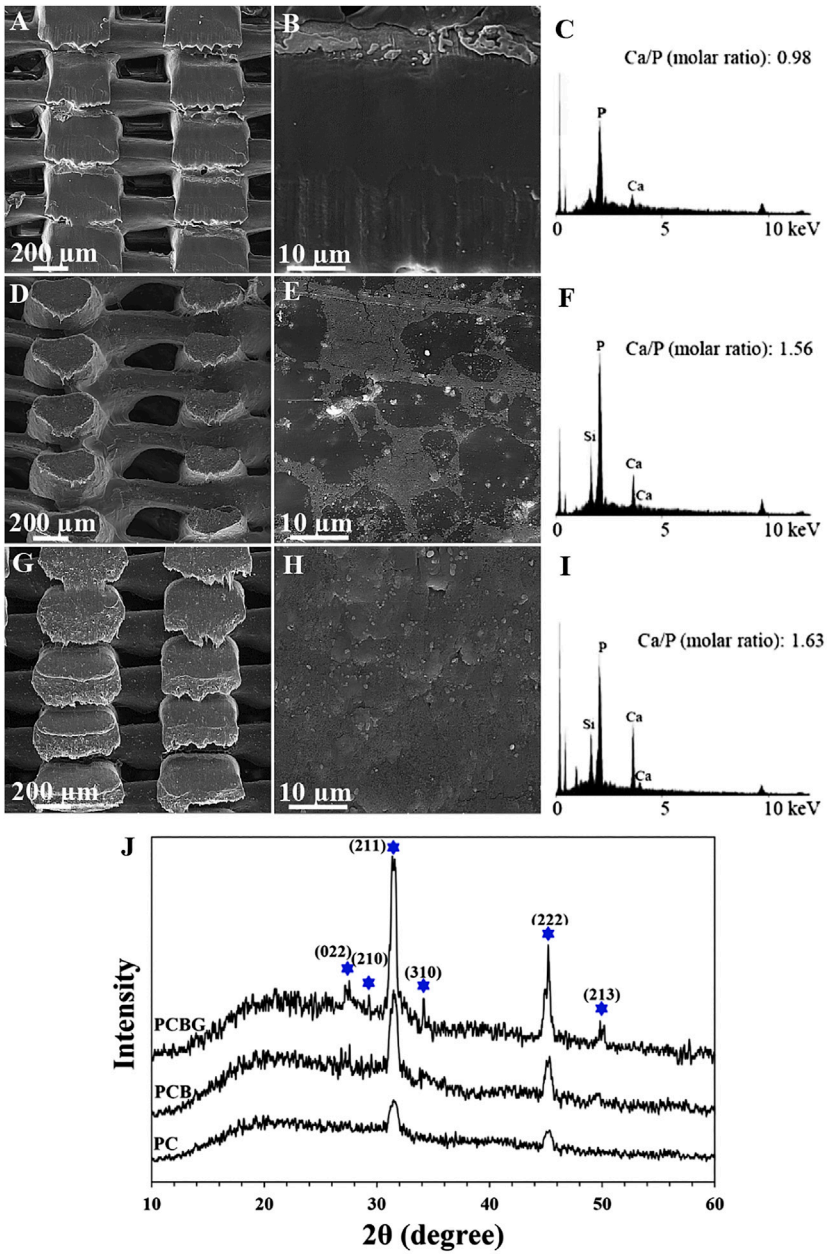

FIGURE 6 | FE-SEM micrographs **(A)**, **(B)**, **(D)**, **(E)**, **(G)**, and **(H)**, EDX spectra **(C)**, **(F)**, and **(I)**, and XRD spectra **(J)** of precipitated hydroxyapatite on the surface of PC **(A)**–**(C)**, PC **(D)**–**(F)**, and PCBG **(G)**–**(I)** matrixes after 4 weeks immersion in the SBF solution.

on the surface of PCBG constructs, such as amide and hydroxyl groups, can be responsible for hybridization in aqueous media (Xing et al., 2014) as well as a significant increment in the mass-loss rate. Additionally, PCBG matrixes showed a lower biodegradation compared with PC matrixes; however, there were no significant differences between the obtained values. Although the modified scaffolds demonstrated a higher hydrophilicity in comparison with PC constructs, the higher compressive strength of PCBG scaffolds could result in consistent stability and a lower degradation. Furthermore, the role of UV irradiation on cross-linking the GelMA layer, improving its stability, and preventing a sudden collapse of the structure should not be ignored (Wang et al., 2014).

Biodegradation of scaffolds and biocompatibility of by-products are concerning issues in tissue engineering. PCL is a semi-crystalline and aliphatic polyester that has shown a degree of resistance to hydrolytic biodegradation, due to its hydrophobic chemical structure (Mahmoud and Salama, 2016). Accordingly, the interconnected tubular pores can support fluid diffusion, provide hydrolysis sites, and possibly the occurrence of biodegradation. Since PCL has both crystalline and amorphous phases, a controllable biodegradation can be observed that

prevents the structure from suddenly collapsing. In fact, the high tendency of the amorphous phase leads to the degradation of these sections, and after that, the crystalline sections will be destroyed (Howard, 2002); therefore, the structure keeps its stability to complete the degradation process. Under the *in-vivo* conditions, acidic by-products originated from the biodegradation of PCL start autocatalytic reactions and accelerate the weight loss rate (Anderson and Shive, 2012). Besides, some organic components such as BGNPs will be degraded by releasing the ions. Herein, depolymerizing of the Si-O-Si bridge will occur after releasing Na^+ in the chemical composition of BGNPs. Consequently, this phenomenon increases the release of Si, Sr, and Ca ions and continues the degradation process (Murphy et al., 2010; Wu et al., 2010a). Additionally, amide and hydroxyl functional groups in the chemical composition of GelMA provide active sites for the rapid chain hydrolyzing (Hosseini et al., 2017) and structure biodegradation.

Bioactivity

In the case of bone tissue engineering, the potential of scaffolds to interact with body fluid ions and the formation of hydroxyapatite-like layers is crucial. To fulfill this purpose, the addition of the bioactive components can be a good strategy. **Figures 6A–I** illustrates the FESEM-EDX results after the immersion of PC, PCB, and PCBG scaffolds after 28 days from immersion in the SBF solution. According to the FE-SEM images, few sediments can be observed on the surface of the PC scaffolds, while BGNPs-contained constructs showed a higher density of the precipitated particles. Additionally, the functionalized scaffolds could also promote biomineralization, since the surface of the strand was entirely and homogeneously covered with nano-scale minerals. EDX analysis proved the presence of calcium and phosphate in the precipitated layers. Moreover, the other elements with a low intensity were detected owing to the sedimentation of SBF ions on the surface (Shuai et al., 2013). The calcium to phosphorus ratio in the PCBG scaffolds showed the nearest ratio to physiological hydroxyapatite (Ca/p = 1.67) compared with PCB and PC scaffolds, which can be considered as an indicator of hydroxyapatite formation. The slight differences in the obtained ratio compared with biological hydroxyapatite may be caused by a lack of carbonate in the chemical composition of the precipitated layer, as observed by Cui et al. in their study (Cui et al., 2016). XRD spectra were also evaluated to ensure the exact composition of the biomineralized calcium phosphate layers. Accordingly, **Figure 6J** indicates the XRD spectra of the 3D-printed scaffolds. A broad peak at 2θ angles around 10–30° arises from the amorphous structure of the applied polymers. The observation of hydroxyapatite characteristic peaks at 2θ angles of 25.27, 27.27, 31.55, 39.65, 45.62, and 49.53° corresponded to the reflection of (002), (210), (211), (310), (222), and (213) crystals (Yaoke et al., 2018). The results indicate that the intensity of hydroxyapatite-related peaks increased after the addition of BGNPs to PCL. Moreover, the modification of the surface with GelMA improved the biomineralization potential through a higher capacity for diffusion of the SBF solution and enrichment of the surface with negatively charged functional groups.

BGNPs provide active sites for the biomimetic formation of calcium phosphates. The formed calcium phosphate layers make the attachment of scaffolds to surrounding tissue possible and also facilitates bone healing (Jo et al., 2009). Herein, sodium and calcium ions in the chemical composition of bioglass are responsible for starting the precipitation of calcium phosphates through replacing the mentioned ions by H^+ in the SBF solution. Finally, the result of this phenomenon will be the release of Si $(OH)_4$. The formation of silanol groups and breakdown of Si-O-Si linkage keep the BGNPs network structure and prevent its dissolution. After the condensation and polymerization of SiO_2, a $CaO\text{-}P_2O_5$ layer would be formed that facilitates the absorption of calcium ions (Hench, 1991). Therefore, the balance in the ionic concentration of the SBF solution would be disturbed, and the surface charge of constructs would be changed. Accordingly, phosphate ions tend to be absorbed on the surface and an interphase of octa calcium phosphate will be formed. Absorption of the other ions in the SBF solution, crystalline hydroxyapatite will cover the surface (Araújo et al., 2015). Besides the effectiveness of BGNPs on calcium and phosphate ions absorption, negatively charged functional groups of GelMA can accelerate the biomineralization process through electrostatic attraction that leads to a reduction in system energy (Li et al., 2008; Kaynak Bayrak et al., 2017.)

Cell-Scaffold Interactions

Before any *in-vivo* observation and cell culture experiments, a fast, simple, and reproducible procedure is necessary to estimate the possible behavior of scaffolds in animals or the human body (Wu et al., 2010b). Accordingly, in this study, the *in-vitro* behavior of scaffolds in the interaction with cells and their potential to support cell adhesion, proliferation, and osteogenic differentiation has been evaluated. The previous investigations have proven that a porous microstructure is required to supply fluid transfer, oxygenation, angiogenesis, and finally, new tissue ingrowth. Accordingly, it is expected that 3D-printed scaffolds with controlled pore characteristics make favorable microenvironments for cellular performance and functionalization (Wu et al., 2010b).

Figures 7A–C illustrates the FE-SEM micrographs of 3D-printed scaffolds after a 3-days culture of BMSCs. Based on the obtained results, the synthetic matrixes could support cell adhesion and spreading originating from the biocompatibility of the applied materials; suitable porosity; and pore size for nutrition, oxygen, and waste materials flow (Gupta et al., 2009). Also, the tubular pore structure of 3D-printed scaffolds can be introduced as an effective factor for ameliorating cell activity (Georgiou et al., 2013). According to the FE-SEM images, although the addition of BGNPs to PCL showed some adverse effects on the hydrophilicity of the constructs, as an important factor in cellular performance, the cell could better adhere to the surface than PC scaffolds that may originate from being provided with the required anchorage site by BGNPs. Fabbri et al. (Fabbri et al., 2010) also indicated a positive role of BGNPs in cellular

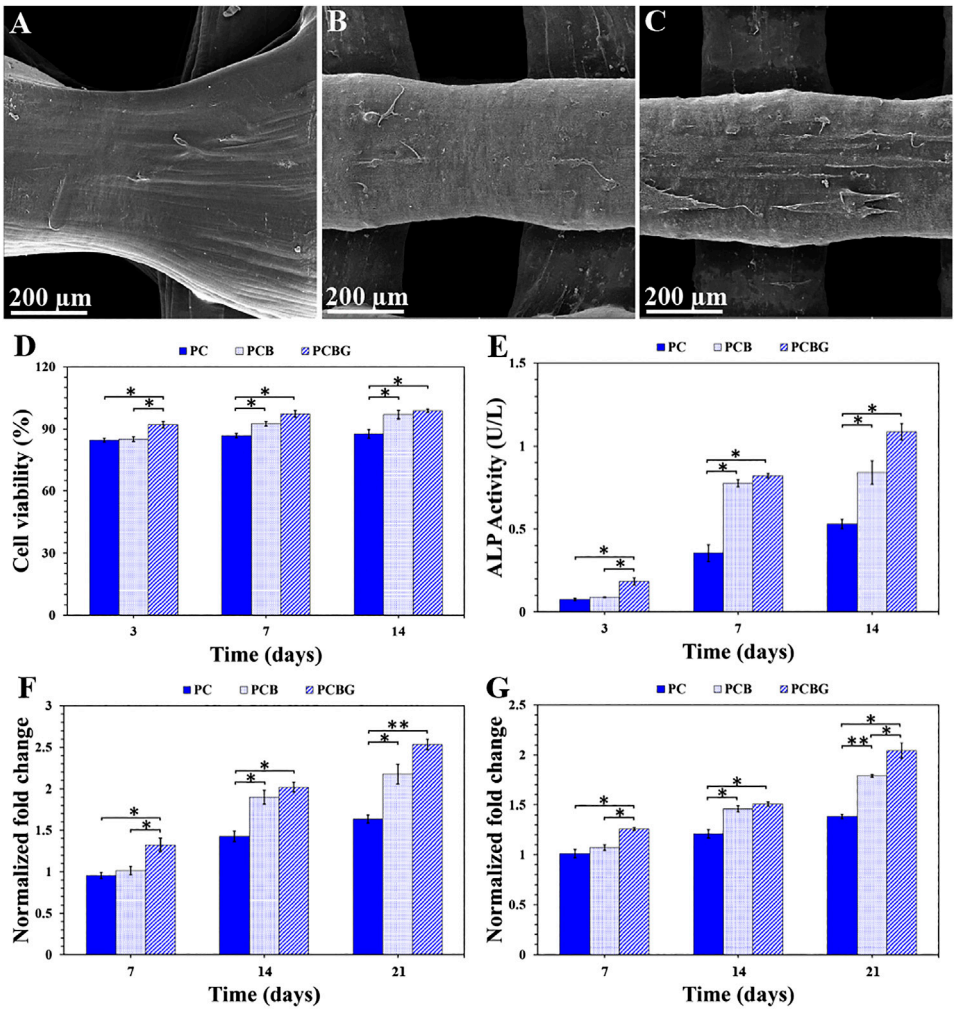

FIGURE 7 | BMSCs adhesion on the surface of PC **(A)**, PCB **(B)**, and PCBG **(C)** scaffolds after a 3-days culture. Cell viability **(D)** and ALP expression **(E)** after cell culture on the surface of 3D-printed constructs within 3, 7, and 14 days. OC **(F)** and OP **(G)** level using quantitative RT-PCR after cell culture on the surface of matrixes for 7, 14, and 21 days. Differences are considered to be statistically significant (*$p < 0.05$) and very statistically significant (**$p < 0.005$).

behavior. Additionally, the functionalized surface with GelMA indicated the promoted cell spreading, density, and pseudopodia formation. In this regard, undoubtedly, the hydrophilicity of GelMA, the improved cell signaling, more interaction with integrin and serum proteins like fibronectin, and low antigenicity are responsible for this observation (Liu et al., 2015).

In this study, the viability of the BMSCs cultured on PC, PCB, and PCBG scaffolds for 14 days, was measured by MTT assay, as indicated in **Figure 7D**. Accordingly, all the test groups showed a desirable biocompatibility owing to the viability of a high number of the cells. Based on the measured values, the number of viable cells has increased as a function of time, showing that the cells can be proliferated on the synthetic substrate. Presumably, nutrient-rich media, better cellular respiration, and low applied stress are responsible for the viability and proliferation of the cells. In a study by Guerra et al. (Guerra et al., 2018) on PCL-based scaffolds, which was printed with 3D printing technology, it was shown that they positively affect the proliferation of 3T3 cells. The addition of BGNPs to PCL scaffolds indicated no significant differences in the number of living cells within 3 days, while it was significantly enhanced in both 7 and 14 days after culture. This observed phenomenon may be due to the release of Si ions from BGNPs that can postpone cell growth (Ghorbani et al., 2018a), but the modification of the surface by a polymeric layer can control and reduce Si release, and a lower influence on cell proliferation can also be observed. Shamsabadi et al. (Shahin-Shamsabadi et al., 2018) proved the formation of elongated filopodia and the spread of cells in the BGNPs-contained structures. In addition, Gabbai-Armelin et al. (Gabbai-Armelin et al., 2015) demonstrated that changing the pH and cell microenvironment during the dissolution of the BGNPs will have a positive effect on the proliferation of the cells. After 3 days of culture, some significant differences were observed between PCBG scaffolds and other test groups, but improving the cellular performance of cells on the PCB scaffold led to the

observation of no statistically significant differences between PCBG and PCB matrixes.

In the case of bone regeneration, osteogenic differentiation of the cells is considered as a crucial factor. Herein, the osteogenic potential of the cultured cells on the surface of 3D-printed scaffolds was evaluated by measuring the level of activity of ALP as well as the expression of OC and OP proteins. Also, the ALP activity, initially an expressed bone marker in osteogenesis (Mandair et al., 2019), is presented in **Figure 7E**. According to the measured values, the higher level of ALP activity has been measured as a function of culture time enhancement. ALP can be observed in post-proliferation, and the ECM maturation procedure and presence of a bioactive component in the chemical composition of scaffolds can promote it (Ge et al., 2014). It was shown that, the addition of BGNPs affects cell differentiation, the production of bone protein, and the expression of ALP (Lin and Fu, 2016). Additionally, other literature introduced BGNPs as osteodifferentiative factors due to the high concentration of silicate ions in the chemical composition (Shahin-Shamsabadi et al., 2018). Furthermore, mitogenic simulation by Si ions resulted in known BGNPs as osteoproductive material. Although Si ions in BGNPs and postponing the cell proliferation led to a delay in gene expression, by passing 7 days from culture, significant differences were observed in the ALP level between PC and PCB constructs. The modified constructs with GelMA followed an incremental slope in ALP activity that may arise from the improved cell proliferation, hydrophilicity, and the interaction with integrin and serum proteins originating from GelMA (Liu et al., 2015).

The expressions of OC and OP nano-collagenous proteins, which are major osteogenic biomarkers and indicators of bone formation, are indicated in **Figures 7F and 7G**, respectively. Accordingly, OC protein is a promoter for the mineralization, which is usually expressed in bone and calcific cartilage, while OP protein is responsible for adjusting adhesion and differentiation of osteoblasts and osteocytes (Krok-Borkowicz et al., 2019). According to the results, in all the test groups, an increase was observed in mRNA expression within 21 days. Notably, the expression of both OC and OP proteins can be an indicator of mineralization potential. However, in this study, OC protein showed a higher level of expression compared with OP protein. Similar to the ALP expression trend, the addition of BGNPs improved the expressions of both OC and OP proteins, while the osteogenic activity was ameliorated after surface modification with GelMA. The observed results reveal that the prepared modified scaffolds have the potential for osteoblastic expression and reconstruction of injured bone.

CONCLUSION

In this study, PCL scaffolds, which were printed with FDM technology, were incorporated with BGNPs, and the surface of constructs was modified by GelMA under UV irradiation to create efficient constructs for bone regeneration. According to the observations, interconnected porous scaffolds with tubular pores were formed in this technology while pore size was increased and strand width was decreased after the addition of BGNPs and surface modification had no particular effect on pore characteristics while they increased the roughness parameters. Besides, mechanical strength was enhanced as a function of BGNPs addition and surface modification. The functionalization of the surface improves hydrophilicity and the absorption capacity of the constructs while higher biodegradation was observed compared with unmodified ones. The potential of scaffolds to support the biomimetic formation of hydroxyapatite was the strength of scaffolds so that the Ca/P ratio of precipitated hydroxyapatite showed the highest degree of similarity to physiological hydroxyapatite after the modification of GelMA on the surface. Additionally, the scaffolds could provide a substrate for adhesion, proliferation, and osteogenic expression of the BMSCs. ALP activity and the expression of OC and OP proteins determined the potential for the reconstruction of injured bone.

DATA AVAILABILITY STATEMENT

All datasets generated for this study are included in the article/supplementary material.

AUTHOR CONTRIBUTIONS

Ideas and the evolution of overarching goals, development and creation of models, conducting an investigation process, specifically data collection and analysis, presentation of the research work, and preparation of the manuscript were done by FG. MS and ZN cooperated in the data collection and analysis procedures. DL was responsible for coordinating the activity planning. Leadership responsibility for the activity planning and execution, including external mentorship to the core team and acquisition of the financial support for the project leading to this publication were performed by BY and AZ.

FUNDING

This work was supported by the Natural Science Foundation of China (Grant No. 81971753), program for medical key department of shanghai (Grant No. ZK2019C01), the Outstanding Clinical Discipline Project of Shanghai Pudong (Grant No. PWYgy2018–09), the Key Disciplines Group Construction Project of Pudong Health Bureau of Shanghai (Grant No. PWZxq2017–11), and the Program for Outstanding Leader of Shanghai (Grant No. 046).

REFERENCES

Anderson, J. M. and Shive, M. S. (2012). Biodegradation and biocompatibility of PLA and PLGA microspheres. *Adv. Drug Delivery Rev.* 64, 72–82. doi:10.1016/j.addr.2012.09.004

Araújo, M., Miola, M., Bertone, E., Baldi, G., Perez, J., and Verné, E. (2015). On the mechanism of apatite-induced precipitation on 45S5 glass pellets coated with a natural-derived polymer. *Appl. Surf. Sci.* 353, 137–149. doi:10.1016/j.apsusc.2015.06.088

Bertassoni, L. E., Cardoso, J. C., Manoharan, V., Cristino, A. L., Bhise, N. S., Araujo, W. A., et al. (2014). Direct-write bioprinting of cell-laden methacrylated gelatin hydrogels. *Biofabrication.* 6, 024105. doi:10.1088/1758-5082/6/2/024105

Boccaccini, A. R. and Ma, P. X. (2014). *Tissue engineering using ceramics and polymers.* Sawston, United Kingdom: Woodhead Publishing Limited, 728.

Chen, Y.-W., Shen, Y.-F., Ho, C.-C., Yu, J., Wu, Y.-H. A., Wang, K., et al. (2018). Osteogenic and angiogenic potentials of the cell-laden hydrogel/mussel-inspired calcium silicate complex hierarchical porous scaffold fabricated by 3D bioprinting. *Mater. Sci. Eng. C.* 91, 679–687. doi:10.1016/j.msec.2018.06.005

Correia, T. R., Ferreira, P., Vaz, R., Alves, P., Figueiredo, M. M., Correia, I. J., et al. (2016). Development of UV cross-linked gelatin coated electrospun poly(caprolactone) fibrous scaffolds for tissue engineering. *Int. J. Biol. Macromol.* 93, 1539–1548. doi:10.1016/j.ijbiomac.2016.05.045

Cui, J., Ma, C., Li, Z., Wu, L., Wei, W., Chen, M., et al. (2016). Polydopamine-functionalized polymer particles as templates for mineralization of hydroxyapatite: biomimetic and in vitro bioactivity. *RSC Adv.* 6, 6747–6755. doi:10.1039/c5ra24821c

De Giglio, E., Bonifacio, M. A., Ferreira, A. M., Cometa, S., Ti, Z. Y., Stanzione, A., et al. (2018). Multi-compartment scaffold fabricated via 3D-printing as *in vitro* co-culture osteogenic model. *Sci. Rep.* 8, 15130. doi:10.1038/s41598-018-33472-1

Deville, S. (2017). *Freezing colloids: observations, principles, control, and use.* Manhattan, NY: Springer International Publishing, 598.

Ding, Y., Li, W., Correia, A., Yang, Y., Zheng, K., Liu, D., et al. (2018). Electrospun polyhydroxybutyrate/poly(ε-caprolactone)/sol-gel-derived silica hybrid scaffolds with drug releasing function for bone tissue engineering applications. *ACS Appl. Mater. Interfaces.* 10, 14540–14548. doi:10.1021/acsami.8b02656

Drago, L., Toscano, M., and Bottagisio, M. (2018). Recent evidence on bioactive glass antimicrobial and antibiofilm activity: a mini-review. *Materials.* 11, 326. doi:10.3390/ma11020326

Fabbri, P., Cannillo, V., Sola, A., Dorigato, A., and Chiellini, F. (2010). Highly porous polycaprolactone-45S5 Bioglass scaffolds for bone tissue engineering. *Compos. Sci. Technol.* 70, 1869–1878. doi:10.1016/j.compscitech.2010.05.029

Gabbai-Armelin, P. R., Souza, M. T., Kido, H. W., Tim, C. R., Bossini, P. S., Magri, A. M. P., et al. (2015). Effect of a new bioactive fibrous glassy scaffold on bone repair. *J. Mater. Sci. Mater. Med.* 26, 1–13. doi:10.1007/s10856-015-5516-1

Garcia Garcia, A., Hébraud, A., Duval, J.-L., Wittmer, C. R., Gaut, L., Duprez, D., et al. (2018). Poly(ε-caprolactone)/Hydroxyapatite 3D honeycomb scaffolds for a cellular microenvironment adapted to maxillofacial bone reconstruction. *ACS Biomater. Sci. Eng.* 4, 3317–3326. doi:10.1021/acsbiomaterials.8b00521

Ge, L., Li, Q., Huang, Y., Yang, S., Ouyang, J., Bu, S., et al. (2014). Polydopamine-coated paper-stack nanofibrous membranes enhancing adipose stem cells' adhesion and osteogenic differentiation. *J. Mater. Chem. B.* 2, 6917–6923. doi:10.1039/C4TB00570H

Georgiou, M., Bunting, S. C. J., Davies, H. A., Loughlin, A. J., Golding, J. P., and Phillips, J. B. (2013). Engineered neural tissue for peripheral nerve repair. *Biomaterials.* 34, 7335–7343. doi:10.1016/j.biomaterials.2013.06.025

Ghorbani, F., Zamanian, A., Behnamghader, A., and Daliri Joupari, M. (2018a). A novel pathway for *in situ* synthesis of modified gelatin microspheres by silane coupling agents as a bioactive platform. *J. Appl. Polym. Sci.* 135, 46739. doi:10.1002/app.46739

Ghorbani, F., Zamanian, A., Behnamghader, A., and Joupari, M. D. (2018b). Microwave-induced rapid formation of biomimetic hydroxyapatite coating on gelatin-siloxane hybrid microspheres in 10X-SBF solution. *e-Polymers.* 18, 247–255. doi:10.1515/epoly-2017-0196

Ghorbani, F. and Zamanian, A. (2018). Oxygen-plasma treatment-induced surface engineering of biomimetic polyurethane nanofibrous scaffolds for gelatin-heparin immobilization. *e-Polymers.* 18, 275–285. doi:10.1515/epoly-2017-0185

Hull, C. (1986). *Apparatus for production of three-dimensional object by stereolithography.* U.S. Patent No US4575330A.

Guerra, A., Cano, P., Rabionet, M., Puig, T., and Ciurana, J. (2018). 3D-Printed PCL/PLA composite stents: towards a new solution to cardiovascular problems. *Materials.* 11, 1679. doi:10.3390/ma11091679

Gupta, D., Venugopal, J., Prabhakaran, M. P., Dev, V. R. G., Low, S., Choon, A. T., et al. (2009). Aligned and random nanofibrous substrate for the *in vitro* culture of Schwann cells for neural tissue engineering. *Acta Biomater.* 5, 2560–2569. doi:10.1016/j.actbio.2009.01.039

Gutta, R., Baker, R. A., Bartolucci, A. A., and Louis, P. J. (2009). Barrier membranes used for ridge augmentation: is there an optimal pore size? *J. Oral Maxillofac. Surg.* 67, 1218–1225. doi:10.1016/j.joms.2008.11.022

Hajiali, F., Tajbakhsh, S., and Shojaei, A. (2018). Fabrication and properties of polycaprolactone composites containing calcium phosphate-based ceramics and bioactive glasses in bone tissue engineering: a review. *Polym. Rev.* 58, 164–207. doi:10.1080/15583724.2017.1332640

Heidari, S., Hooshmand, T., Yekta, B. E., Tarlani, A., Noshiri, N., and Tahriri, M. (2018). Effect of addition of titanium on structural, mechanical and biological properties of 45S5 glass-ceramic. *Ceram. Int.* 44, 11682–11692. doi:10.1016/j.ceramint.2018.03.245

Hench, L. L. (1991). Bioceramics: from concept to clinic. *J. Am. Ceram. Soc.* 74, 1487–1510. doi:10.1111/j.1151-2916.1991.tb07132.x

Hench, L. L. (2015). The future of bioactive ceramics. *J. Mater. Sci. Mater. Med.* 26, 1–4. doi:10.1007/s10856-015-5425-3

Hench, L. L., Wheeler, D. L., and Greenspan, D. C. (1998). Molecular control of bioactivity in sol-gel glasses. *J. Sol. Gel Sci. Technol.* 13, 245–250. doi:10.1023/A:1008643303888

Hidalgo Pitaluga, L., Trevelin Souza, M., Dutra Zanotto, E., Santocildes Romero, M., and Hatton, P. (2018). Electrospun F18 bioactive glass/PCL-poly (ε-caprolactone)-Membrane for guided tissue regeneration. *Materials.* 11, 400. doi:10.3390/ma11030400

Hong, Z., Reis, R. L., and Mano, J. F. (2008). Preparation and *in vitro* characterization of scaffolds of poly(l-lactic acid) containing bioactive glass ceramic nanoparticles. *Acta Biomater.* 4, 1297–1306. doi:10.1016/j.actbio.2008.03.007

Hosseini, Y., Emadi, R., and Kharaziha, M. (2017). Surface modification of PCL-diopside fibrous membrane via gelatin immobilization for bone tissue engineering. *Mater. Chem. Phys.* 194, 356–366. doi:10.1016/j.matchemphys.2017.03.051

Howard, G. T. (2002). Biodegradation of polyurethane: a review. *Int. Biodeterior. Biodegrad.* 49, 245–252. doi:10.1016/S0964-8305(02)00051-3

Huang, A., Peng, X., Geng, L., Zhang, L., Huang, K., Chen, B., et al. (2018). Electrospun poly (butylene succinate)/cellulose nanocrystals bio-nanocomposite scaffolds for tissue engineering: preparation, characterization and *in vitro* evaluation. *Polym. Test.* 71, 101–109. doi:10.1016/j.polymertesting.2018.08.027

Jeon, H. J., Lee, M., Yun, S., Kang, D., Park, K. H., Choi, S., et al. (2019). Fabrication and characterization of 3D-printed biocomposite scaffolds based on PCL and silanated silica particles for bone tissue regeneration. *Chem. Eng. J.* 360, 519–530. doi:10.1016/j.cej.2018.11.176

Jo, J. H., Lee, E. J., Shin, D. S., Kim, H. E., Kim, H. W., Koh, Y. H., et al. (2009). In vitro/in vivo biocompatibility and mechanical properties of bioactive glass nanofiber and poly(epsilon-caprolactone) composite materials. *J. Biomed. Mater. Res. B Appl. Biomater.* 91, 213–220. doi:10.1002/jbm.b.31392

Jones, J. R., Kemp, T. F., and Smith, M. E. (2006). Effect of OH content on the bioactivity of sol-gel derived glass foam scaffolds. *Key Eng. Mater.* 309, 1031–1034. doi:10.4028/www.scientific.net/kem.309-311.1031

Jose, M., Thomas, V., Johnson, K., Dean, D., and Nyairo, E. (2009). Aligned PLGA/HA nanofibrous nanocomposite scaffolds for bone tissue engineering. *Acta Biomater.* 5, 305–315. doi:10.1016/j.actbio.2008.07.019

Kaynak Bayrak, G., Demirtaş, T. T., and Gümüşderelioğlu, M. (2017). Microwave-induced biomimetic approach for hydroxyapatite coatings of chitosan scaffolds. *Carbohydr. Polym.* 157, 803–813. doi:10.1016/j.carbpol.2016.10.016

Khatiwala, C. B., Peyton, S. R., Metzke, M., and Putnam, A. J. (2007). The regulation of osteogenesis by ECM rigidity in MC3T3-E1 cells requires MAPK activation. *J. Cell. Physiol.* 211, 661–672. doi:10.1002/jcp.20974

Kiernan, C. H., Wolvius, E. B., Brama, P. A. J., and Farrell, E. (2017). The immune response to allogeneic differentiated mesenchymal stem cells in the context of bone tissue engineering, *Tissue Eng. Part B Rev.* 24, 75. doi:10.1089/ten.TEB.2017.0175

Kokubo, T. (2008). *Bioceramics and their clinical applications.* Sawston, United Kingdom: Woodhead Publishing Limited.

Korpela, J., Kokkari, A., Korhonen, H., Malin, M., Närhi, T., and Seppälä, J. (2013). Biodegradable and bioactive porous scaffold structures prepared using fused deposition modeling. *J. Biomed. Mater. Res. B Appl. Biomater.*, 101, 610–619. doi:10.1002/jbm.b.32863

Krok-Borkowicz, M., Filova, E., Chlupac, J., Klepetar, J., Bacakova, L., and Pamuła, E. (2019). Influence of pore size and hydroxyapatite deposition in poly(l-lactide-co-glycolide) scaffolds on osteoblast-like cells cultured in static and dynamic conditions. *Mater. Lett.* 241, 1–5. doi:10.1016/j.matlet.2019.01.039

Lee, K. Y., Alsberg, E., Hsiong, S., Comisar, W., Linderman, J., Ziff, R., et al.(2004). Nanoscale Adhesion ligand organization regulates osteoblast proliferation and differentiation. *Nano Lett.* 4, 1501–1506. doi:10.1021/nl0493592

Lee, S., Choi, D., Shim, J.-H., and Nam, W. (2020). Efficacy of three-dimensionally printed polycaprolactone/beta tricalcium phosphate scaffold on mandibular reconstruction. *Sci. Rep.* 10, 4979. doi:10.1038/s41598-020-61944-w

Li, X., Xie, J., Yuan, X., and Xia, Y. (2008). Coating electrospun poly(epsilon-caprolactone) fibers with gelatin and calcium phosphate and their use as biomimetic scaffolds for bone tissue engineering. *Langmuir.* 24, 14145–14150. doi:10.1021/la802984a

Lin, C.-C. and Fu, S.-J. (2016). Osteogenesis of human adipose-derived stem cells on poly(dopamine)-coated electrospun poly(lactic acid) fiber mats. *Mater. Sci. Eng. C.* 58, 254–263. doi:10.1016/j.msec.2015.08.009

Lin, Y.-H. H., Chiu, Y.-C. C., Shen, Y.-F. F., Wu, Y.-H. A. H. A., and Shie, M.-Y. Y. (2018). Bioactive calcium silicate/poly-ε-caprolactone composite scaffolds 3D printed under mild conditions for bone tissue engineering. *J. Mater. Sci. Mater. Med.* 29, 11. doi:10.1007/s10856-017-6020-6

Liu, S., Hsueh, C., Wen-Neng Ueng, S., Lin, S., and Chen, J. (2009). Manufacture of solvent-free polylactic-glycolic acid (PLGA) scaffolds for tissue engineering. *Asia-Pac. J. Chem. Eng.* 4, 154–160. doi:10.1002/apj.187

Liu, M., Zhou, J., Yang, Y., Zheng, M., Yang, J., and Tan, J. (2015). Surface modification of zirconia with polydopamine to enhance fibroblast response and decrease bacterial activity *in vitro*: a potential technique for soft tissue engineering applications. *Colloids Surf. B Biointerfaces.* 136, 74–83. doi:10.1016/j.colsurfb.2015.06.047

Liu, J., Li, L., Suo, H., Yan, M., Yin, J., and Fu, J. (2019). 3D printing of biomimetic multi-layered GelMA/nHA scaffold for osteochondral defect repair. *Mater. Des.* 171, 107708. doi:10.1016/j.matdes.2019.107708

Long, T., Yang, J., Shi, S. S., Guo, Y. P., Ke, Q. F., and Zhu, Z. A. (2015). Fabrication of three-dimensional porous scaffold based on collagen fiber and bioglass for bone tissue engineering. *J. Biomed. Mater. Res. B Appl. Biomater.* 103, 1455–1464. doi:10.1002/jbm.b.33328

Ma, Z., He, W., Yong, T., and Ramakrishna, S. (2005). Grafting of gelatin on electrospun poly(caprolactone) nanofibers to improve endothelial cell spreading and proliferation and to control cell orientation. *Tissue Eng.* 11, 1149–1158. doi:10.1089/ten.2005.11.1149

Mahmoud, A. A. and Salama, A. H. (2016). Norfloxacin-loaded collagen/chitosan scaffolds for skin reconstruction: preparation, evaluation and in-vivo wound healing assessment. *Eur. J. Pharm. Sci.* 83, 155–165. doi:10.1016/j.ejps.2015.12.026

Mandair, G. S., Steenhuis, P., Ignelzi, M. A., and Morris, M. D. (2019). Bone quality assessment of osteogenic cell cultures by Raman microscopy. *J. Raman Spectrosc.* 50, 360–370. doi:10.1002/jrs.5521

Miszuk, J. M., Xu, T., Yao, Q., Fang, F., Childs, J. D., Hong, Z., et al. (2018). Functionalization of PCL-3D electrospun nanofibrous scaffolds for improved BMP2-induced bone formation. *Appl. Mater. Today.* 10, 194–202. doi:10.1016/j.apmt.2017.12.004

Murphy, S., Wren, A. W., Towler, M. R., and Boyd, D. (2010). The effect of ionic dissolution products of Ca-Sr-Na-Zn-Si bioactive glass on *in vitro* cytocompatibility. *J. Mater. Sci. Mater. Med.* 21, 2827–2834. doi:10.1007/s10856-010-4139-9

Nandagiri, V. K., Gentile, P., Chiono, V., Tonda-Turo, C., Matsiko, A., Ramtoola, Z., et al. (2011). Incorporation of PLGA nanoparticles into porous chitosan-gelatin scaffolds: influence on the physical properties and cell behavior. *J. Mech. Behav. Biomed. Mater.* 4, 1318–1327. doi:10.1016/j.jmbbm.2011.04.019

Oki, A., Parveen, B., Hossain, S., Adeniji, S., and Donahue, H. (2004). Preparation and in vitro bioactivity of zinc containing sol-gel-derived bioglass materials. *J. Biomed. Mater. Res. A.* 69, 216–221. doi:10.1002/jbm.a.20070

Pan, Z. and Ding, J. (2012). Poly(lactide-co-glycolide) porous scaffolds for tissue engineering and regenerative medicine. *Interface Focus.* 2, 366–377. doi:10.1098/rsfs.2011.0123

Park, H., Cho, H.-H., Kim, K., Hong, K., Kim, J.-H., Choe, H., et al. (2018a). Surface-oxidized, freeze-cast cobalt foams: microstructure, mechanical properties and electrochemical performance. *Acta Mater.* 142, 213–225. doi:10.1016/j.actamat.2017.09.066

Park, J. U., Jeong, S. H., Song, E. H., Song, J., Kim, H. E., and Kim, S. (2018b). Acceleration of the healing process of full-thickness wounds using hydrophilic chitosan-silica hybrid sponge in a porcine model. *J. Biomater. Appl.* 32, 1011–1023. doi:10.1177/0885328217751246

Park, S. A., Lee, S. J., Seok, J. M., Lee, J. H., Kim, W. D., and Kwon, I. K. (2018c). Fabrication of 3D printed PCL/PEG polyblend scaffold using rapid prototyping system for bone tissue engineering application. *J. Bionic Eng.* 15, 435–442. doi:10.1007/s42235-018-0034-8

Pati, F., Song, T.-H., Rijal, G., Jang, J., Won, S., Cho, D., et al. (2015). Ornamenting 3D printed scaffolds with cell-laid extracellular matrix for bone tissue regeneration. *Biomaterials.* 37, 230–241. doi:10.1016/j.biomaterials.2014.10.012

Pourhaghgouy, M., Zamanian, A., Shahrezaee, M., and Masouleh, M. P. (2016). Physicochemical properties and bioactivity of freeze-cast chitosan nanocomposite scaffolds reinforced with bioactive glass. *Mater. Sci. Eng. C.* 58, 180–186. doi:10.1016/j.msec.2015.07.065

Prabha, R. D., Kraft, D. C. E., Harkness, L., Melsen, B., Varma, H., Nair, P. D., et al. (2018). Bioactive nano-fibrous scaffold for vascularized craniofacial bone regeneration. *J. Tissue Eng. Regen. Med.* 12, e1537–e1548. doi:10.1002/term.2579

Rindone, A. N., Nyberg, E., and Grayson, W. L. (2017). 3D-Printing composite polycaprolactone-decellularized bone matrix scaffolds for bone tissue engineering applications. *Methods Mol. Biol.* 1577, 209–226. doi:10.1007/7651_2017_37

Salmoria, G. V., Pereira, R. V., Fredel, M. C., and Casadei, A. P. M. (2018). Properties of PLDLA/bioglass scaffolds produced by selective laser sintering. *Polym. Bull.* 75, 1299–1309. doi:10.1007/s00289-017-2093-0

Shahin-Shamsabadi, A., Hashemi, A., Tahriri, M., Bastami, F., Salehi, M., and Mashhadi Abbas, F. (2018). Mechanical, material, and biological study of a PCL/bioactive glass bone scaffold: importance of viscoelasticity. *Mater. Sci. Eng. C.* 90, 280–288. doi:10.1016/j.msec.2018.04.080

Sharifi, E., Azami, M., Kajbafzadeh, A. M., Moztarzadeh, F., Faridi-Majidi, R., Shamousi, A., et al. (2016). Preparation of a biomimetic composite scaffold from gelatin/collagen and bioactive glass fibers for bone tissue engineering. *Mater. Sci. Eng. C.* 59, 533–541. doi:10.1016/j.msec.2015.09.037

Shen, H., Hu, X., Yang, F., Bei, J., and Wang, S. (2007). Combining oxygen plasma treatment with anchorage of cationized gelatin for enhancing cell affinity of poly(lactide-co-glycolide). *Biomaterials.* 28, 4219–4230. doi:10.1016/j.biomaterials.2007.06.004

Shuai, C., Zhuang, J., Hu, H., Peng, S., Liu, D., and Liu, J. (2013). In vitrobioactivity and degradability of β-tricalcium phosphate porous scaffold fabricated via selective laser sintering. *Biotechnol. Appl. Biochem.* 60, 266–273. doi:10.1002/bab.1064

Siri, S., Wadbua, P., Amornkitbamrung, V., Kampa, N., and Maensiri, S. (2010). Surface modification of electrospun PCL scaffolds by plasma treatment and addition of adhesive protein to promote fibroblast cell adhesion. *Mater. Sci. Technol.* 26, 1292–1297. doi:10.1179/026708310x12798718274070

Su, M., Gu, A., Liang, G., and Yuan, L. (2011). The effect of oxygen-plasma treatment on Kevlar fibers and the properties of Kevlar fibers/bismaleimide composites. *Appl. Surf. Sci.* 257, 3158–3167. doi:10.1016/j.apsusc.2010.10.133

Tan, Y., Richards, D. J., Trusk, T. C., Visconti, R. P., Yost, M. J., Kindy, M. S., et al. (2014). 3D printing facilitated scaffold-free tissue unit fabrication. *Biofabrication.* 6, 024111. doi:10.1088/1758-5082/6/2/024111

Thomas, C. H., Collier, J. H., Sfeir, C. S., and Healy, K. E. (2002). Engineering gene expression and protein synthesis by modulation of nuclear shape. *Proc. Natl. Acad. Sci.* 99, 1972–1977. doi:10.1073/pnas.032668799

Tonda-Turo, C., Gentile, P., Saracino, S., Chiono, V., Nandagiri, V. K., Muzio, G., et al. (2011). Comparative analysis of gelatin scaffolds crosslinked by genipin and silane coupling agent. *Int. J. Biol. Macromol.* 49, 700–706. doi:10.1016/j.ijbiomac.2011.07.002

Tsai, W. B., Chen, W. T., Chien, H. W., Kuo, W. H., and Wang, M. J. (2011). Poly(dopamine) coating of scaffolds for articular cartilage tissue engineering. *Acta Biomater.* 7, 4187–4194. doi:10.1016/j.actbio.2011.07.024

Unnithan, A. R., Sasikala, A. R. K., Murugesan, P., Gurusamy, M., Wu, D., Park, C. H., et al. (2015). Electrospun polyurethane-dextran nanofiber mats loaded with Estradiol for post-menopausal wound dressing. *Int. J. Biol. Macromol.* 77, 1–8. doi:10.1016/j.ijbiomac.2015.02.044

Videau, J. J. and Dupuis, V. (1991). Phosphates and biomaterials. *Eur. J. Solid State Inorg. Chem.* 28, 303–343.

Wang, H., Zhou, L., Liao, J., Tan, Y., Ouyang, K., Ning, C., et al. (2014). Cell-laden photocrosslinked GelMA-DexMA copolymer hydrogels with tunable mechanical properties for tissue engineering. *J. Mater. Sci. Mater. Med.* 25, 2173–2183. doi:10.1007/s10856-014-5261-x

Wang, Z., Kumar, H., Tian, Z., Jin, X., Holzman, J. F., Menard, F., et al. (2018). Visible light photoinitiation of cell-adhesive gelatin methacryloyl hydrogels for stereolithography 3D bioprinting. *ACS Appl. Mater. Interfaces.* 10, 26859–26869. doi:10.1021/acsami.8b06607

Wang, L., Xu, W., Chen, Y., and Wang, J. (2019a). Alveolar bone repair of rhesus monkeys by using BMP-2 gene and mesenchymal stem cells loaded three-dimensional printed bioglass scaffold. *Sci. Rep.* 9, 18175. doi:10.1038/s41598-019-54551-x

Wang, X., Molino, B. Z., Pitkänen, S., Ojansivu, M., Xu, C., Hannula, M., et al. (2019b). 3D scaffolds of polycaprolactone/copper-doped bioactive glass: architecture engineering with additive manufacturing and cellular assessments in a coculture of bone marrow stem cells and endothelial cells. *ACS Biomater. Sci. Eng.* 5, 4496–4510. doi:10.1021/acsbiomaterials.9b00105

Wu, W., Geng, P., Li, G., Zhao, D., Zhang, H., and Zhao, J. (2015). Influence of layer thickness and raster angle on the mechanical properties of 3D-printed PEEK and a comparative mechanical study between PEEK and ABS. *Materials.* 8, 5834–5846. doi:10.3390/ma8095271

Kim, C., Zhu, Y., Chang, J., Zhang, Y., and Xiao, Y. (2010a). Bioactive inorganic-materials/alginate composite microspheres with controllable drug-delivery ability. *J. Biomed. Mater. Res. B Appl. Biomater.* 94, 32–43. doi:10.1002/jbm.b.31621

Wu, X., Liu, Y., Li, X., Wen, P., Zhang, Y., Long, Y., et al. (2010b). Preparation of aligned porous gelatin scaffolds by unidirectional freeze-drying method. *Acta Biomater.* 6, 1167–1177. doi:10.1016/j.actbio.2009.08.041

Xiang, P., Wang, S. S., He, M., Han, Y. H., Zhou, Z. H., Chen, D. L., et al. (2018). The in vitro and in vivo biocompatibility evaluation of electrospun recombinant spider silk protein/PCL/gelatin for small caliber vascular tissue engineering scaffolds. *Colloids Surf. B Biointerfaces.* 163, 19–28. doi:10.1016/j.colsurfb.2017.12.020

Xing, Q., Yates, K., Vogt, C., Qian, Z., Frost, M. C., and Zhao, F. (2014). Increasing mechanical strength of gelatin hydrogels by divalent metal ion removal. *Sci. Rep.* 4, 4706–4716. doi:10.1038/srep04706

Yan, Y., Wang, X., Pan, Y., Liu, H., Cheng, J., Xiong, Z., et al. (2005). Fabrication of viable tissue-engineered constructs with 3D cell-assembly technique. *Biomaterials.* 26, 5864–5871. doi:10.1016/j.biomaterials.2005.02.027

Yang, C., Tian, X., Li, D., Cao, Y., Zhao, F., and Shi, C. (2017). Influence of thermal processing conditions in 3D printing on the crystallinity and mechanical properties of PEEK material. *J. Mater. Process. Technol.* 248, 1–7. doi:10.1016/j.jmatprotec.2017.04.027

Yaoke, D., Yuan, Z., and Wang, J. (2018). Synthesis of a phosphorus-containing trisilanol POSS and its application in RTV composites. *e-Polymers.* 18, 237–245. doi:10.1515/epoly-2017-0204

Yetiskin, B. and Okay, O. (2019). High-strength and self-recoverable silk fibroin cryogels with anisotropic swelling and mechanical properties. *Int. J. Biol. Macromol.* 122, 1279–1289. doi:10.1016/j.ijbiomac.2018.09.087

Yin, J., Yan, M., Wang, Y., Fu, J., and Suo, H. (2018). 3D bioprinting of low-concentration cell-laden gelatin methacrylate (GelMA) bioinks with a two-step cross-linking strategy. *ACS Appl. Mater. Interfaces.* 10, 6849–6857. doi:10.1021/acsami.7b16059

Ylänen, H. (2017). *Bioactive glasses: materials, properties and applications.* Sawston, United Kingdom: Woodhead Publishing Limited.

Yue, K., Trujillo-de Santiago, G., Alvarez, M. M., Tamayol, A., Annabi, N., and Khademhosseini, A. (2015). Synthesis, properties, and biomedical applications of gelatin methacryloyl (GelMA) hydrogels. *Biomaterials.* 73, 254–271. doi:10.1016/j.biomaterials.2015.08.045

Zahedi Tehrani, T., Bagheri Cheimeh, M., Ebrahimi-Barough, S., Azami, M., Shirian, S., Atyabi, S. M., et al. (2018). Comparison of cell proliferation and adhesion of human osteoblast differentiated cells on electrospun and freeze-dried PLGA/bioglass scaffolds. *Arch. Neurosci.* 5. doi:10.5812/ans.67266

Zein, I., Hutmacher, D. W., Tan, K. C., and Teoh, S. H. (2002). Fused deposition modeling of novel scaffold architectures for tissue engineering applications. *Biomaterials.* 23, 1169–1185. doi:10.1016/S0142-9612(01)00232-0

Zhang, J., Zhao, S., Zhu, M., Zhu, Y., Zhang, Y., Liu, Z., et al. (2014). 3D-printed magnetic Fe3O4/MBG/PCL composite scaffolds with multifunctionality of bone regeneration, local anticancer drug delivery and hyperthermia. *J. Mater. Chem. B.* 2, 7583–7595. doi:10.1039/c4tb01063a

Zhu, Y., Gao, C., He, T., and Shen, J. (2004). Endothelium regeneration on luminal surface of polyurethane vascular scaffold modified with diamine and covalently grafted with gelatin. *Biomaterials.* 25, 423–430. doi:10.1016/S0142-9612(03)00549-0

Conflict of Interest: The authors declare that the research was conducted in the absence of any commercial or financial relationships that could be construed as a potential conflict of interest.

Copyright © 2020 Ghorbani, Sahranavard, Mousavi Nejad, Li, Zamanian and Yu. This is an open-access article distributed under the terms of the Creative Commons Attribution License (CC BY). The use, distribution or reproduction in other forums is permitted, provided the original author(s) and the copyright owner(s) are credited and that the original publication in this journal is cited, in accordance with accepted academic practice. No use, distribution or reproduction is permitted which does not comply with these terms.